Tissue-specific extracellular matrix scaffolds for the regeneration of spatially complex musculoskeletal tissues

Gráinne M. Cunniffe [a, b, c, 1], Pedro J. Díaz-Payno [a, b, 1], Eamon J. Sheehy [a, b, d], Susan E. Critchley [a, b], Henrique V. Almeida [a, b], Pierluca Pitacco [a, b], Simon F. Carroll [a, b], Olwyn R. Mahon [a, b, e], Aisling Dunne [e], Tanya J. Levingstone [c, d], Conor J. Moran [c, d], Robert T. Brady [c, d], Fergal J. O'Brien [a, b, c, d], Pieter A.J. Brama [f], Daniel J. Kelly [a, b, c, d, *]

[a] Trinity Centre for Bioengineering, Trinity Biomedical Sciences Institute, Trinity College Dublin, Dublin, Ireland.
[b] Department of Mechanical and Manufacturing Engineering, School of Engineering, Trinity College Dublin, Dublin, Ireland.
[c] Advanced Materials and Bioengineering Research Centre (AMBER), Royal College of Surgeons in Ireland and Trinity College Dublin, Dublin, Ireland.
[d] Tissue Engineering Research Group, Department of Anatomy, Royal College of Surgeons in Ireland, Dublin, Ireland.
[e] Molecular Immunology Group, School of Biochemistry and Immunology, Trinity College Dublin, Dublin, Ireland.
[f] School of Veterinary Medicine, University College Dublin, Dublin, Ireland.

[1] These authors contributed equally.

* Corresponding author at: Department of Mechanical and Manufacturing Engineering, School of Engineering, Trinity College Dublin, Dublin 2, Ireland. Tel.: +353 1 896 3947; fax: +353 1 679 5554. E-mail address: kellyd9@tcd.ie

---

https://doi.org/10.1016/j.biomaterials.2018.09.044

Received 31 July 2018; Received in revised form 18 September 2018; Accepted 28 September 2018

Biomaterials 188 (2019) 63–73

Available online 04 October 2018

Keywords

Extracellular matrix; Scaffold; Growth plate; Articular cartilage; Osteochondral defect

Abstract

Biological scaffolds generated from tissue-derived extracellular matrix (ECM) are commonly used clinically for soft tissue regeneration. Such biomaterials can enhance tissue-specific differentiation of adult stem cells, suggesting that structuring different ECMs into multi-layered scaffolds can form the basis of new strategies for regenerating damaged interfacial tissues such as the osteochondral unit. In this study, mass spectrometry is used to demonstrate that growth plate (GP) and articular cartilage (AC) ECMs contain a unique array of regulatory proteins that may be particularly suited to bone and cartilage repair respectively. Applying a novel iterative freeze-drying method, porous bi-phasic scaffolds composed of GP ECM overlaid by AC ECM are fabricated, which are capable of spatially directing stem cell differentiation *in vitro*, promoting the development of graded tissues transitioning from calcified cartilage to hyaline-like cartilage. Evaluating repair 12-months post-implantation into critically-sized caprine osteochondral defects reveals that these scaffolds promote regeneration in a manner distinct to commercial control-scaffolds. The GP layer supports endochondral bone formation, while the AC layer stimulates the formation of an overlying layer of hyaline cartilage with a collagen fiber architecture better recapitulating the native tissue. These findings support the use of a bi-layered, tissue-specific ECM derived scaffolds for regenerating spatially complex musculoskeletal tissues.

Graphical abstract

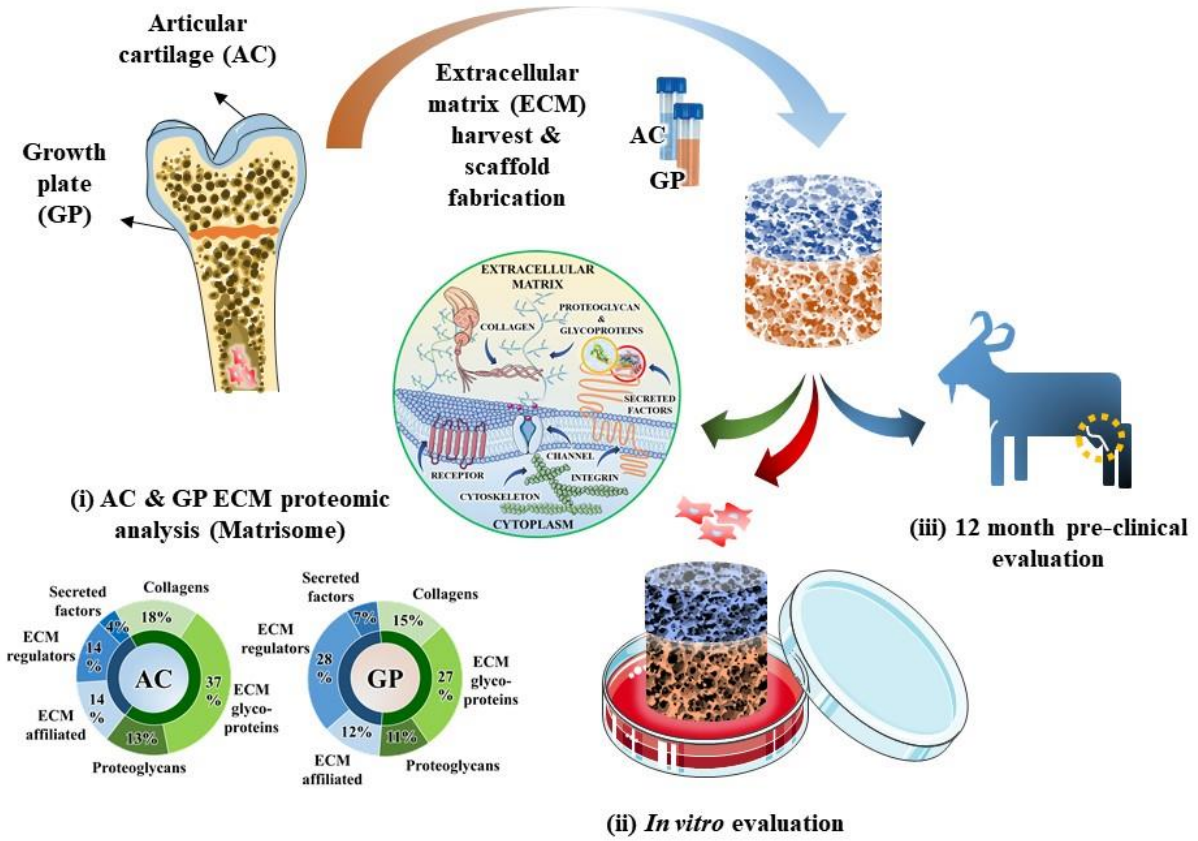

1. Introduction

Extracellular matrix (ECM) derived biomaterials have been used clinically over 1 million times in the surgical repair of different tissues and organs [1–5]. While the exact mechanism by which these bioactive scaffolds promote regeneration remains unclear, in the early stages of healing, the ECM supports the development of a pro-regenerative immune response involving both the adaptive and the innate immune system [6]. In particular, a favorable regenerative outcome has been linked to a ratio of M2 (anti-inflammatory) to M1 (pro-inflammatory) macrophages that facilitates tissue remodeling [7]. Scaffolds used clinically are typically derived from small intestine submucosa (SIS) or pericardium, and while the ECM of these tissues clearly contain structural and regulatory biomolecules generally supportive of regeneration [8], it is unlikely

that a single tissue source of ECM will be optimal for all clinical targets. This concept is strengthened by recent studies reporting that ECM derived biomaterials can direct the differentiation of mesenchymal stem cells (MSCs) towards the phenotype of the source tissue from which they were derived [9–11]. This motivates the development of tissue-specific ECM derived scaffolds, potentially consisting of different layers or lineage-specific regions [12–14], especially when attempting to regenerate complex multi-phasic tissues such as the osteochondral unit of synovial joints. Articular cartilage possesses a poor regenerative capacity, with tissue damage typically progressing across the joint surface and into the underlying subchondral bone. If left untreated, these osteochondral defects can progress to osteoarthritis of the joint, motivating the need for new regenerative strategies to repair damaged synovial joints.

Cartilaginous tissues play key roles in the development and function of the musculoskeletal system. The epiphyseal plate or growth plate (GP), a cartilaginous tissue in the metaphysis at each end of a developing long bone, is responsible for its longitudinal growth through a coordinated process of endochondral ossification (*the replacement of cartilage with bone*). Articular cartilage (AC), a form of hyaline cartilage, lines the ends of bones within synovial joints and functions to provide a smooth, low-friction surface for articulation and to facilitate the transmission of load across the joint. The ECM of both GP and AC have been successfully used to produce scaffolds for tissue engineering, with GP derived biomaterials shown to support large bone defect healing [15–17], and AC derived scaffolds shown to support chondrogenesis [9,18,19]. To better understand their regenerative potential, we first compared the proteome of solubilized GP and AC, demonstrating that they contain a unique array of regulatory factors potentially important to bone and cartilage regeneration. Furthermore, porous scaffolds derived from these two ECMs supported the development of distinct tissue types when seeded with MSCs. Based on these findings, we hypothesized that a bi-phasic

scaffold consisting of spatially distinct but integrated layers of GP and AC ECM could be used to regenerate osteochondral defects. This study describes the capacity of these scaffolds to spatially direct MSC differentiation *in vitro* and the mechanism by which they can direct joint repair *in vivo* following their cell-free implantation in critically-sized caprine osteochondral defects.

2. Material and methods

2.1. Tissue harvest and scaffold fabrication

Articular cartilage (AC) and growth plate (GP) ECM tissues were harvested from porcine hind limbs (3-4 months old), purchased from a local abattoir shortly after sacrifice. The AC was obtained from the femoral head using a biopsy punch. Subsequently, the head of the bone was split open using a saw to reveal the epiphyseal line and to gain access to the GP, which was then carefully extracted using a scalpel. The AC and GP tissues were separately pulverized using a cryomiller (SPEX SamplePrep®, NJ, USA), whereby liquid nitrogen was used to freeze the samples before mechanically grinding (3 x 1 min cycles) to create ECM powders. These powders were then re-suspended to form AC and GP slurries at 500 mg/ml in ddH_2O. Slurries were freeze-dried to generate AC and GP scaffolds for initial *in vitro* characterization, as previously described [9,20] (Φ5 x h3 mm). Briefly, the slurry temperature was reduced to −30 °C (1 °C/min) and maintained for 1 h to allow for ice-crystal nucleation and growth. The temperature was then increased to −10 °C (1 °C/min), followed by a hold of 24 h to allow for sublimation of the frozen water, and then finally increased to room temperature (0.5 °C/min). Scaffolds then underwent dehydrothermal crosslinking (DHT) in a vacuum oven (VD23, Binder, Germany), at 105 °C, at 0.5 mbar for 24 h. For the bi-layered scaffolds a novel, iterative freezing step was introduced. The GP slurry was firstly frozen within custom-made

polydimethylsiloxane (PDMS) cylindrical molds to -20 ºC (1°C/min) before an upper layer of AC slurry was added and subsequently frozen (AC-GP scaffolds prepared for *in vitro* analysis: Φ5 x h1.5 mm each layer, total height 3 mm; for *in vivo* evaluation AC layer: Φ6 x h2 mm and GP layer: Φ6 x h4 mm, total height 6 mm) before undergoing lyophilization and DHT as described above. Scaffolds were imaged using scanning electron microscopy (SEM) following fixation, alcohol dehydration and gold-palladium coating and pore size was calculated using Image J.

2.2. Protein analysis

ECM powders were treated with 6M Guanidine-hydrochloride for protein extraction [21]. Precipitation of soluble proteins was done using trichloroacetic (TCA) solution, acetone, 6 M urea in 50 mM ammonium bicarbonate (ABC) followed by treatment in 5 mM dithiothreitol (DTT) at 60 °C for 30 min, 10 mM iodoacetamide (IAA) at room temperature for 30 min and trypsin digestion prior to mass spectrometry analysis and western blot details. The samples were run on a Thermo Scientific Q Exactive mass spectrometer connected to a Dionex Ultimate 3000 (RSLCnano) chromatography system. Tryptic peptides were resuspended in formic acid. Each sample was loaded onto a fused silica emitter (75 μm ID, pulled using a laser puller (Sutter Instruments P2000)), packed with UChrom C18 (1.8 μm) reverse phase media (nanoLCMS Solutions LCC) and was separated by an increasing acetonitrile gradient over 45/60 minutes at a flow rate of 250 nL/min. The mass spectrometer was operated in positive ion mode with a capillary temperature of 320 °C, and with a potential of 2300V applied to the frit. All data was acquired with the mass spectrometer operating in automatic data dependent switching mode. A high resolution (70,000) MS scan (300-1600 m/z) was performed using the Q Exactive to select the 8 most intense ions prior to MS/MS analysis using HCD. The raw data was *de novo* sequenced and searched against the *sus scrofa* complete Uniprot database using the search

engine Maxquant [22–24], for peptides cleaved with trypsin. Each peptide used for protein identification met specific Maxquant parameters, i.e. only peptide scores that corresponded to a false discovery rate (FDR) of ≤1% were accepted. Proteins identified by Maxquant were processed with Perseus [25] in order to elucidate differences across the two tissues. MatrisomeDB [26] was used to cluster proteins into subgroups in order to find protein-protein interactions and to identify target molecules of interest.

2.3. In vitro analysis

Bone marrow derived mesenchymal stem cells (MSCs) were harvested following a standard protocol, from porcine hind limbs (3-4 months old), purchased from a local abattoir shortly after sacrifice. MSCs were used at passage 2 and seeded at a density of 500,000 cells per scaffold. Constructs were cultured in chondrogenic medium containing 10 ng/ml transforming growth factor β3 (TGF-β3, R&D Systems®). Cell viability was assessed at day 7 using live/dead staining (2 mM EthD-1 and 5 mM Calcein for 1 h) and confocal microscopy.

2.4. Histological and biochemical analysis

Samples at day 0 and day 28 (n=3) were fixed in 4% paraformaldehyde, dehydrated and wax embedded to allow serial slicing (6 μm) at the center of the constructs. Staining was performed using 1% alcian blue 8GX in 0.1 M HCl, picro-sirius red and alizarin red for evaluation of sGAG, collagen and calcium deposition, respectively. Collagen type II, X, I and VEGF synthesis was evaluated using a standard immunohistochemical technique with the appropriate primary antibody; 1:100 IgG mouse monoclonal anti-collagen type I (ab90395, Abcam®, UK), anti-collagen type II (ab3092, Abcam®, UK), 1:100 IgM mouse monoclonal anti-collagen type X (ab49945, Abcam®, UK) or 1:200 IgG rabbit polyclonal anti-VEGF (ab46154, Abcam®,

UK). Biochemical analysis was also used to supplement histological findings by measuring sGAG (dimethylmethylene blue dye-binding assay from Blyscan, Biocolor Ltd, Northern Ireland), collagen (Chloramine-T assay, hydroxyproline:collagen ratio of 1:7.69 [27]) and calcium content (O-cresolphthalein complexone assay, Sentinel Diagnostics) in papain digested samples (n=3), as previously described [11].

2.5. In vivo implantation

Surgical procedure in caprine model was carried out as previously described [14]. Briefly, the goats were sedated using diazepam (0.3 – 0 .4 mg/kg IV) and butorphanol (0.2 mg/kg IV). An epidural was administered using morphine (0.2 mg/kg). Following placement of an intravenous catheter, anesthesia was induced with propofol (max. dose 4 mg/kg IV). Anesthesia was maintained using isoflurane with ventilation to maintain normal end tidal CO_2 between 4.6 and 6 kPa. Isotonic fluids were provided at 10 ml/kg/h. Following induction of anesthesia, the goats were placed in dorsal recumbency and an arthrotomy of each stifle joint was then performed using the lateral para-patellar approach. A critically-sized defect, 6 mm in diameter x 6 mm in depth, was created in each medial femoral condyle using a hand drill, a flattened drill bit and a depth guide. The joint was flushed with normal fluids (0.9 % NaCl) and the stifle joints were assigned to one of the two treatment groups: 1) Maioregen scaffold (Finceramica), herein called the Control scaffold and 2) AC-GP ECM derived bi-layered scaffold, herein called the AC-GP scaffold. The commercial scaffold was cut to a diameter of 6 mm and to a depth of 6 mm in accordance with the manufacturers' guidelines. Both scaffold types were press fit into the defect site cell-free before routine closure of the joint capsule, subcutaneous tissues and skin. Morphine (0.1 - 0.2 mg/kg IM) and non-steroidal anti-inflammatory drugs (NSAIDs) [Carprofen (1.5 - 2.5 mg/kg subcutaneously) (Rimadyl)] were administered at the end of anesthesia. Following surgery, goats were housed in small indoor pens to allow skin incisions

to heal and were allowed full weight bearing immediately. During this period the animals were closely monitored to ensure adequate analgesia. NSAIDs and antibiotics [Amoxicillin (Noroclav)] were administered for 5 days post-surgery. Two weeks post-operatively, following removal of sutures, animals were let out to pasture for the remainder of the study period. Euthanasia was carried out with an overdose of sodium pentobarbital (Euthatal) administered by I.V. injection at 6 and 12 month time points ($n \geq 6$) to permit harvesting of the treated condyles. Ethical evaluation and approval was administered by University College Dublin (AREC 12-71) and the Irish Government Department of Health (B100/4517).

2.6. Repair tissue evaluation

Macroscopic evaluation of the joints was performed immediately upon opening the joint (Table 1). 1.5 cm^3 sections containing the defect site were harvested, samples were fixed in a formalin solution and the levels of mineralization within the repair tissue (5 mm diameter cylindrical region) was quantified using μCT (Scanco Medical, Switzerland) at a threshold of 210, corresponding to a density of 399.5 mg hydroxyapatite/cm^3. Demineralized wax-embedded constructs were sectioned at 10 μm and stained with safranin O, hematoxylin and eosin and picro-sirius red and immunostained for collagen type II for ICRS evaluation (Fig. S3 and Table S1) [28]. Safranin O staining was also used in combination with Photoshop CS6 to quantify the area of positively stained cartilage within a region of interest (ROI) in the articular cartilage and subchondral bone regions of the repair tissue. Picro-sirius red stained samples were imaged under polarized light microscopy to investigate collagen fiber orientation. Directionality plugin [29] from Image J was used to quantify the mean orientation and angular dispersion of the collagen fibers observed in the superficial and deep zones of the regenerated articular cartilage (Fig. S4).

Table 1. Macroscopic scoring system for cartilage repair. Maximum score possible is 12.

Characteristic	Grading	Score
Degree of defect repair	In level with surrounding cartilage	4
	75 % repair of defect depth	3
	50 % repair of defect depth	2
	25 % repair of defect depth	1
	0 % repair of defect depth	0
Integration to border zone	Complete integration with surrounding cartilage	4
	Demarcating border < 1 mm	3
	¾ implant integrated with surrounding cartilage, ¼ notable border > 1 mm	2
	½ implant integrated with surrounding cartilage, ½ notable border > 1 mm	1
	From ¼ implant integrated to no contact with surrounding cartilage	0
Macroscopic appearance	Intact smooth surface	4
	Fibrillated surface	3
	Small, scattered fissures or cracks	2
	Several, small or few but large fissures	1
	Total degeneration of grafted area	0

2.7. Statistical analysis

All statistical analyses were performed using GraphPad Prism, except for mass spectrometry which was analyzed using Perseus. All values are reported as means ± standard deviation. Significance for all statistical analyses was defined as $p < 0.05$.

3. Results

3.1. Growth plate and articular cartilage contain shared and distinct regulatory proteins

Growth plate (GP) and articular cartilage (AC) ECM from the femur of skeletally immature pigs (Fig. 1a) were found to contain a range of shared and distinct proteins (Table S1 and Table S2). Of the 297 proteins identified within AC, 89% of these were also detected within GP, however, of the 603 proteins detected in the GP tissue, the majority (56%) were not found in AC (Fig. 1b and c). Further bioinformatics analysis and filtering, through MatrisomeDB [26], revealed that the two tissues contained a similar number of core matrisome proteins, including collagens, ECM glycoproteins and proteoglycans (Fig. 1d). The GP tissue, however, contained more abundant matrisome-associated proteins such as ECM-affiliated, ECM regulators, and secreted factors. Of interest was the finding that the GP contained proteins that are believed to play a role in angiogenesis, such as CSPG4 [30,31] and ANGPTL2 [32,33]; and osteogenesis, including CLEC11A [34], MMP13 [35,36] and S100A10 [37,38]. In contrast, AC contained factors known to inhibit hypertrophy and to promote chondrogenesis, such as GREM1, FRZB [39] and TGFβi [40,41]. The differential presence of selected key proteins detected using mass spectrometry were also verified using western blots (Fig. 1e).

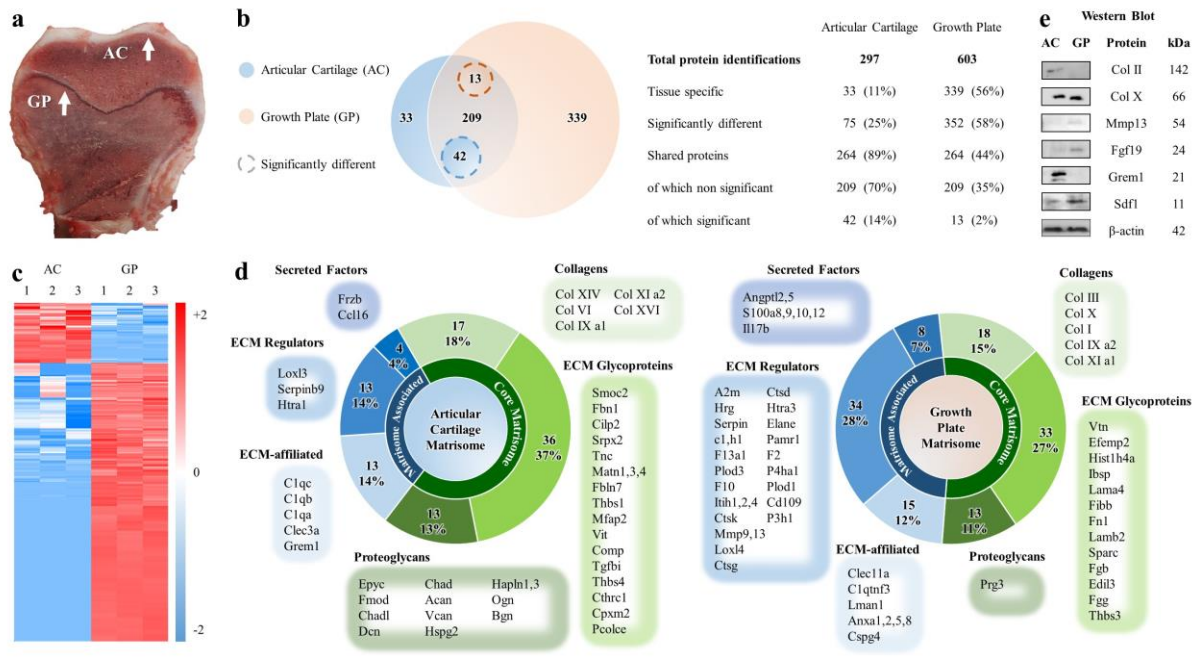

Fig. 1. Comparison of Articular Cartilage (AC) and Growth Plate (GP) ECM proteome. a) Macroscopic image demonstrating the location of the harvested AC and GP ECM within a porcine femur. b) Venn diagram of the total numbers of proteins identified via mass spectrometry which were either specific to, or shared by AC or GP tissues. c) Heat map of the mass spectrometry analysis of soluble factors present within 3 biological replicates of AC and GP tissues. d) Characterization of the total number of proteins detected in each tissue, categorized into core matrisome or matrisome-associated proteins. The listed proteins are the significantly expressed proteins identified in either AC or GP matrisomes, grouped into clusters associated with their structure and function. e) Western blot analysis of key proteins differentially detected in either tissue type.

3.2. AC and GP ECM derived scaffolds promote tissue-specific differentiation of MSCs

Having demonstrated that AC and GP contain distinct protein profiles, we next sought to verify that scaffolds produced using these two ECMs would provide tissue-specific cues to

encapsulated stem cells. Porous scaffolds were fabricated via freeze-drying of a suspension of either AC or GP derived ECM [9,20]. The scaffolds were found to facilitate the infiltration of bone marrow derived MSCs within 24 hours of seeding (Fig. 2a). Pores ranging in size from 10 to 300 μm, with a mean pore size of 109±50 μm for AC and 126 ± 52 μm in GP scaffolds, were observed using SEM (Fig. S1). AC and GP scaffolds seeded with MSCs were then cultured under identical conditions for 28 days in the presence of transforming growth factor (TGF)-β3, with the resultant tissue deposition analyzed to evaluate the osteo- or chondro-inductive properties of the two different scaffolds. While both scaffolds supported the development of a cartilaginous tissue, significantly higher levels of sulphated glycosaminoglycan (sGAG) and collagen were deposited in the AC scaffolds (Fig. 2b and c), suggesting that this biomaterial was more supportive of hyaline cartilage development. In contrast, significantly higher levels of calcium deposition were detected within the GP scaffolds, suggesting that this biomaterial was more osteogenic and supported the development of a calcified cartilage. These apparent phenotypic differences were confirmed by immunohistochemical analysis which demonstrated enhanced deposition of collagen type X, collagen type I and vascular endothelial growth factor (VEGF) within the GP scaffolds, while higher levels of collagen type II deposition were observed within the AC scaffold (Fig. 2d). Taken together, these findings suggest that the GP ECM scaffolds support the development of a VEGF expressing calcified cartilage, while AC ECM derived scaffolds support the development of a hyaline-like cartilage rich in proteoglycans and collagen type II.

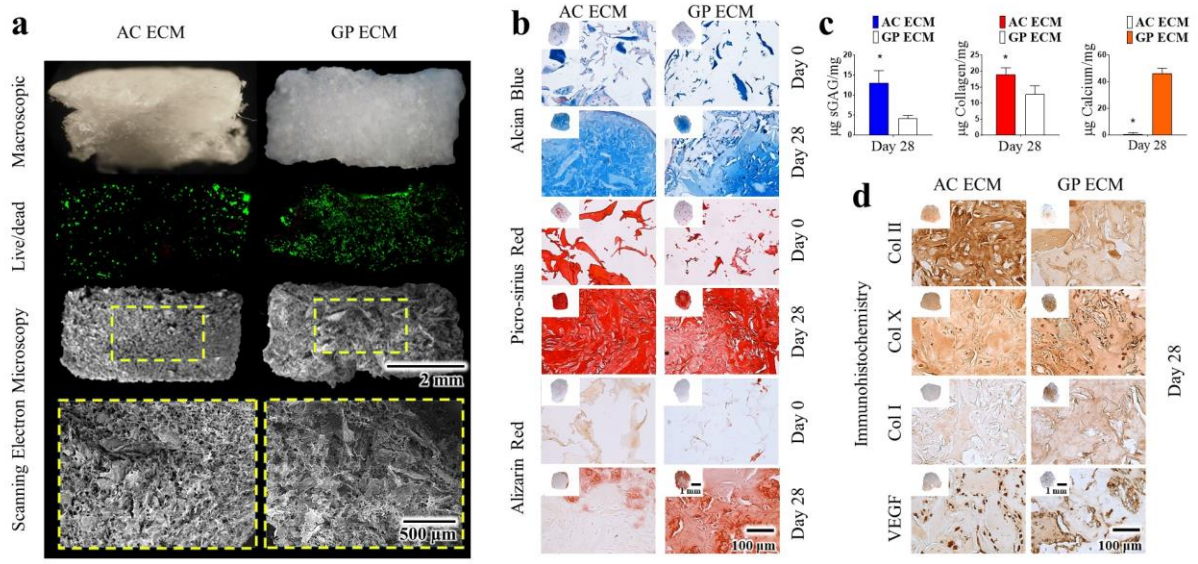

Fig. 2. ECM scaffolds regulate MSC differentiation *in vitro*. a) Macroscopic images of porous, freeze-dried scaffolds formed from either AC or GP ECM; confocal images stained for live/dead analysis of the distribution of MSCs throughout both scaffolds 24 h post-seeding; and SEM images of the scaffolds showing the interconnected pore structure achieved via controlled freeze-drying. b) Histological staining for sulphated glycosaminoglycan (sGAG), collagen and calcium deposition at day 0 and after 28 days in chondrogenic culture conditions. c) Quantification of sGAG, collagen and calcium deposition in each scaffold after 28 days. d) Immunohistochemical staining for collagen type II, collagen type X, collagen type I and VEGF; $^{*}p < 0.05$, ANOVA.

3.3. Bi-layered ECM scaffolds facilitate the development of spatially complex tissues

Using a novel iterative freeze-drying process, AC and GP ECM were next combined to create a bi-layered porous scaffold with distinct but interconnected AC and GP regions (termed 'AC-GP scaffolds'; Fig. 3a). To investigate if these bi-layered AC-GP scaffolds could spatially direct stem cell differentiation based solely on their differential composition, they were seeded

with a single population of MSCs and cultured for 28 days in the presence of TGF-β3. Qualitative and quantitative evaluation of each ECM layer indicated that they were capable of driving tissue-specific stem cell differentiation and matrix deposition, with higher levels of sGAG and collagen deposition observed in the AC layer and higher levels of cartilage matrix calcification observed in the GP layer (Fig. 3b and c). More intense staining for collagen type II was observed within the AC layer of the scaffold, while higher levels of collagen type I and collagen type X accumulated within the GP layer. MSC-mediated deposition of VEGF was also higher in the GP layer of the scaffold (Fig. 3d). Together this data demonstrates that bi-layered AC-GP scaffolds are capable of spatially regulating the differentiation of MSCs to produce a graded tissue that transitions from calcified cartilage to hyaline cartilage.

Successful integration of ECM scaffolds within a defect site is also dependent on eliciting appropriate host immune responses; therefore, before commencing large animal studies preliminary assays were carried out to examine the effect of the different ECMs on the phenotype and secretome of primary human macrophages. It was observed that both ECM scaffolds evoked minimal IL-6, 10 and 12 production. Interestingly, GP ECM scaffolds induced the expression of higher levels of the chemokine IL-8 (Fig. S2), which has previously been shown to promote osteoclastogenesis [42,43]. AC scaffolds enhanced the mRNA expression of basic fibroblast growth factor (bFGF), a growth factor known to enhance chondrogenesis [44], while GP scaffolds enhanced the expression of pro-angiogenic factors VEGF and Angiopoietin 1 (ANG1).

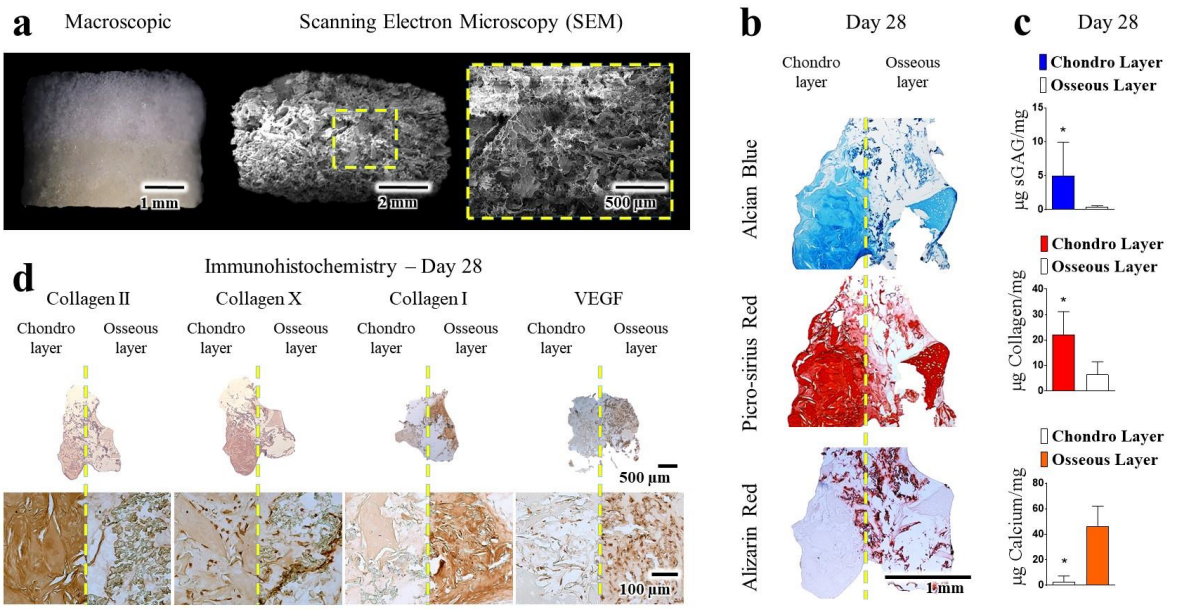

Fig. 3. Bi-layered ECM scaffolds spatially direct MSC differentiation *in vitro*. a) Macroscopic and SEM images of bi-layered AC-GP scaffolds demonstrating the spatial control, seamless interface and the inherent porosity achieved through the iterative freeze-drying procedure. b) Histological images of bi-layered scaffolds seeded with a single population of MSCs and evaluated for the deposition of sGAG, collagen and calcium after 28 days in chondrogenic culture conditions. c) Corresponding quantification of the sGAG, collagen and calcium deposition within each individual layer of the scaffold. d) Immunohistochemical staining for collagen type II, collagen type X, collagen type I and VEGF. *$p < 0.05$, ANOVA.

3.4. Bi-layered ECM derived scaffolds promote host-mediated osteochondral defect regeneration

To evaluate their regenerative potential *in vivo*, bi-layered AC-GP scaffolds were implanted (cell-free) into critically-sized osteochondral defects created in the medial femoral condyles of goats. 6 and 12 months after scaffold implantation, the quality of repair was compared to that produced by implanting a collagen type I-based control scaffold (MaioRegen, Finceramica),

which is currently in human clinical use for osteochondral defect repair [45]. The macroscopic appearance of defects treated with the two scaffolds appeared similar at both time-points (Fig. 4a), with no significant difference in the macroscopic score between the AC-GP scaffold and the control scaffold (Fig. 4a, b). Reconstructing images obtained from μCT scanning of the harvested osteochondral sections also demonstrated good regeneration of the bony region of the osteochondral defects treated with either scaffold (Fig. 4c). The bone volume within the subarticular spongiosa region of the defect (SAS; defined as the bottom 3 mm of the bony region of the defect) significantly increased between 6 and 12 months in defects treated with the AC-GP scaffolds, but not with the control scaffold (Fig. 4d). Bone volume in the subchondral bone plate (SBP; defined as the upper 1 mm of the bony region of the defect) was higher than in the subarticular spongiosa, however no significant differences in bone levels were observed between the two scaffolds in this region of the defect. Native bone has a similar bone volume value to the regenerated defects at 12 months (data not shown).

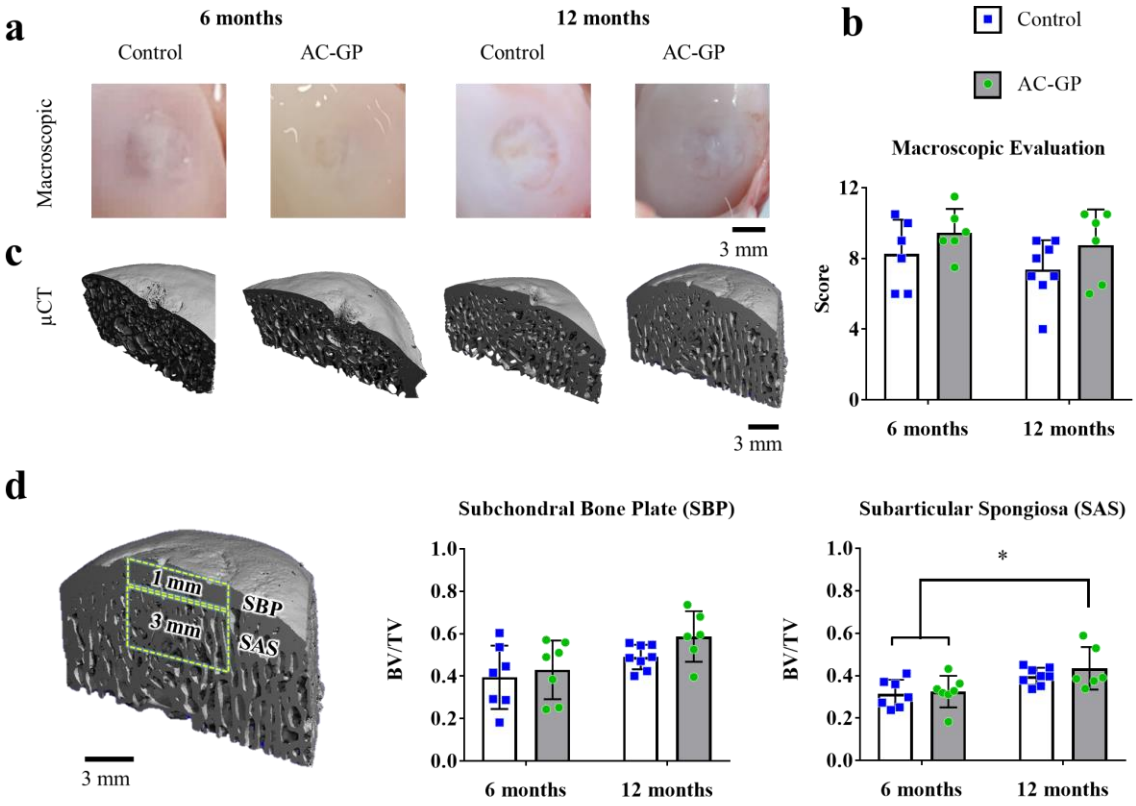

Fig. 4. Macroscopic and bone density analysis of healing within treated caprine osteochondral defects. a) Macroscopic representative images of healing achieved through the treatment of osteochondral defects with control scaffolds or bi-layered AC-GP scaffolds after 6 and 12 months, respectively, and b) quantification of the macroscopic appearance of the defects based on repair tissue integration, % defect fill and chondrogenic appearance. c) Reconstructed µCT images demonstrating the distribution of mineralized tissue across the center of the repair tissue at both time points. d) Quantification of the bone volume per total volume within two regions of the defect, the upper 1 mm subchondral bone plate region and the lower 3 mm subarticular spongiosa region at both time points. *$p < 0.05$, ANOVA.

Examining the repair tissue in more detail using standard histological techniques revealed that the percentage of repair tissue staining positive with safranin-O for proteoglycans (Fig. 5a), an

indicator of cartilage tissue development, was significantly higher in the chondral regions of defects treated with the AC-GP scaffolds after 6 months (Fig. 5b). No significant difference was observed by 12 months (Fig. 5b). A trend towards higher levels of cartilage tissue formation within the subchondral region was observed in defects treated with the AC-GP scaffolds after 6 months, although this was not statistically significant. Cartilage levels within the osseous region of defects treated with the AC-GP scaffolds noticeably decreased between 6 and 12 months, suggesting that regeneration of the osseous region of the defect is occurring, at least in part, by endochondral ossification. The cartilage region of the repair tissue in both groups also stained positive for collagen type II, the predominant type of collagen found in hyaline cartilage (Fig. 5c). By 12 months, a collagen network organization similar to native condyles was detected more consistently in the AC-GP treated defects. The International Cartilage Repair Society (ICRS) scores [28] of these histological sections are provided in Fig. S3, with a trend towards higher "Average Cartilage" scores for the ECM treated group at both time points (6 months: Control 42.32 *vs.* AC-GP 54.52, 12 months: Control 51.14 *vs.* AC-GP 63.26).

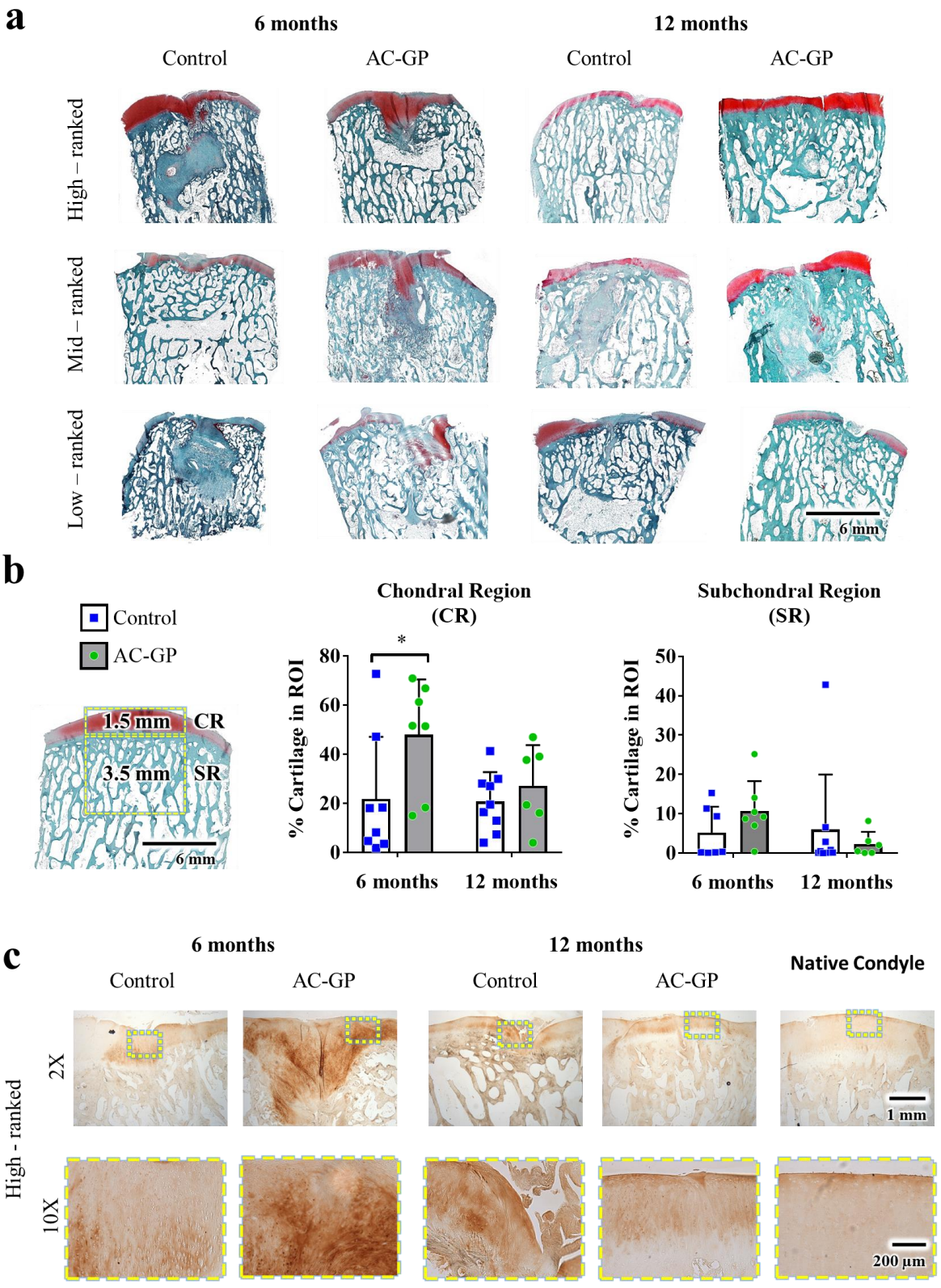

Fig. 5. Analysis of articular cartilage and subchondral bone repair following scaffold implantation. a) Cartilage matrix staining (red, safranin-O) for the highest-, mid- and lowest-

ranked samples at 6 and 12 months, scored blindly using established ICRS scoring methods (Fig. S3 and Table S1). b) Quantification of the percentage of tissue classified as cartilage in the upper chondral region, and in the lower subchondral region of the repair tissue at both time points. c) Collagen type II stained samples for control and AC-GP scaffold treated groups at 2x and 10x magnifications, shown next to a native condyle control. *$p < 0.05$, ANOVA.

Motivated by the histological findings which suggested the development of a more hyaline-like repair tissue in AC-GP scaffold treated defects, the organization of the newly formed collagen fiber network was examined in more detail using polarized light microscopy (PLM) (Fig. 6a), and the predominant angle of orientation and the dispersion of the fiber orientations were quantified in the upper (Top) superficial region, and deep (Bottom) cartilage region (Fig. 6 b and c), using *Directionality* plugin from Image J [29]. At both 6 and 12 months, the collagen fiber organization of the repair tissue within AC-GP treated defects was consistently more similar to native cartilage samples than the control group. A parallel fiber orientation (approaching 0 degrees) with a lower range of dispersion was observed at both time points in the superficial cartilage region of the AC-GP treated defects, while a perpendicular fiber orientation (approaching 90 degrees) was achieved more consistently in the deeper cartilage regions following treatment with the AC-GP scaffold.

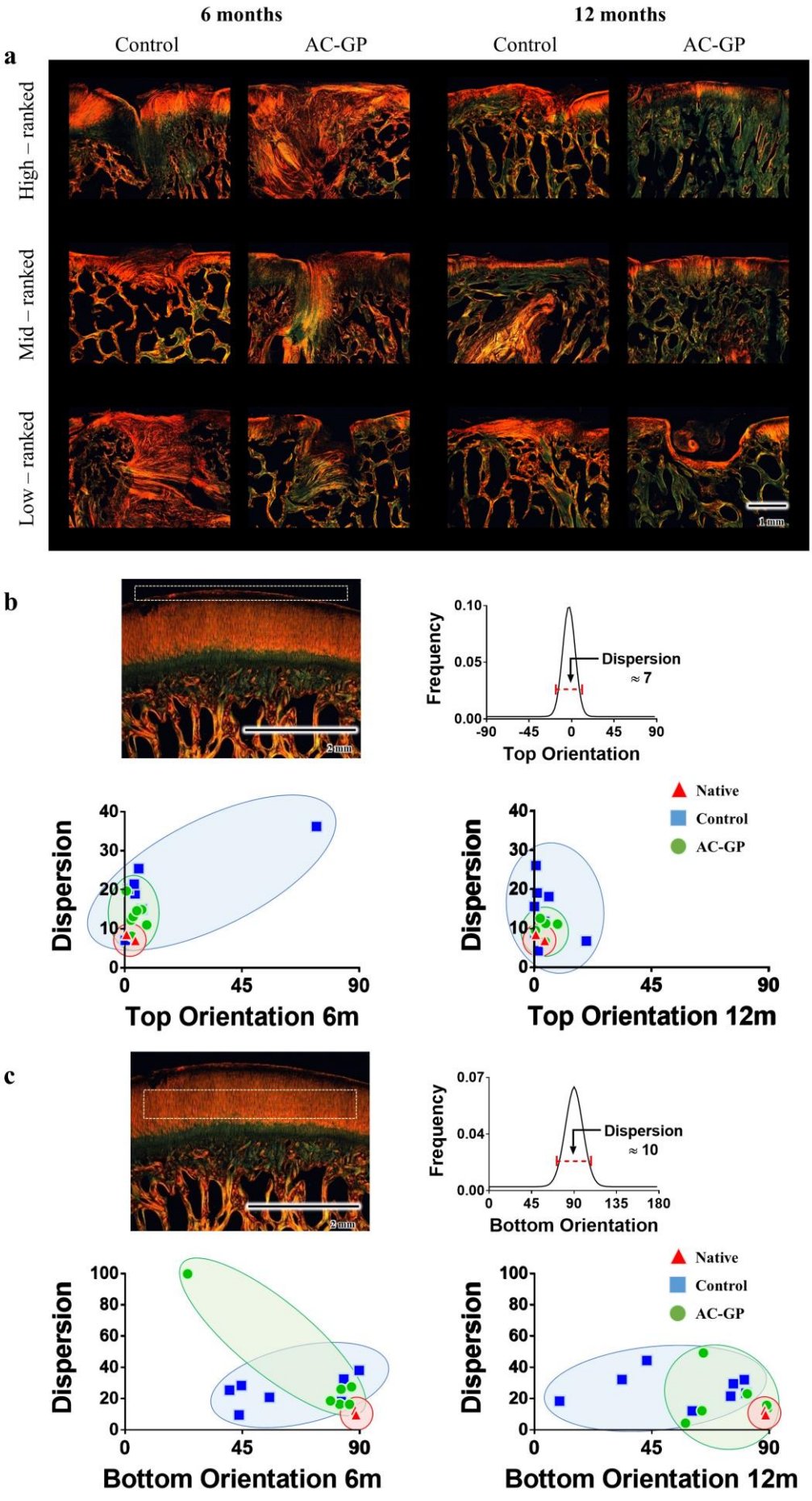
a
6 months
12 months
Control
AC-GP
Control
AC-GP
High – ranked
Mid – ranked
Low – ranked
1 mm
b
2 mm
Frequency
0.10
0.05
0.00
-90
-45
0
45
90
Dispersion
≈ 7
Top Orientation
Dispersion
Top Orientation 6m
Native
Control
AC-GP
Dispersion
Top Orientation 12m
c
2 mm
Frequency
0.07
0.04
0.00
0
45
90
135
180
Dispersion
≈ 10
Bottom Orientation
Dispersion
Bottom Orientation 6m
Native
Control
AC-GP
Dispersion
Bottom Orientation 12m

Fig. 6. Analysis of collagen fiber organization within repaired cartilage. a) PLM images indicating the orientation of the collagen fibers within the repair tissue of control and AC-GP scaffold treated groups at 6 and 12 months. b) Evaluation of the collagen fiber orientation in the superficial (Top) zone and c) deep cartilage (Bottom) zone within the repair tissue relative to a native condyle control at 6 and 12 months. A lower dispersion value indicates a more consistent fiber orientation within the sample. Fibers running parallel to the surface possess an orientation of 0 degrees, while fibers running perpendicular have an orientation of 90 degrees in native articular cartilage tissue.

4. Discussion

The results of this study demonstrate that bi-layered ECM derived scaffolds can direct tissue-specific stem cell differentiation *in vitro* and during regeneration of caprine osteochondral defects. In isolation, GP ECM derived scaffolds supported the development of a calcified cartilage tissue *in vitro,* confirming their potential for endochondral bone regeneration [11]. In contrast, the AC ECM derived scaffolds supported the development of an articular cartilage-like tissue that appeared more resistant to hypertrophy and endochondral ossification. These two ECMs were then combined using a novel freeze-drying technique to produce a bi-layered scaffold, which was found capable of spatially directing the differentiation of single population of MSCs *in vitro,* resulting in the development of a graded tissue that transitioned from calcified cartilage to hyaline-like cartilage. Over 12 months *in vivo,* these bi-layered ECM derived scaffolds promoted a distinct pattern of repair within caprine osteochondral defects, resulting in the regeneration of hyaline cartilage with a collagen fiber architecture that better recapitulated the native tissue compared to commercially available control scaffolds.

In vitro, we found that the different ECM derived scaffolds promoted the development of either calcified or hyaline cartilage following seeding with bone marrow derived MSCs. This can be correlated to the unique composition of each ECM, which was determined based on an in-depth analysis of the less abundant non-collagenous proteins in this tissue. The proteins detected in the GP using mass spectrometry analysis are in agreement with previous studies, confirming that hypertrophic chondrocytes resident in the GP express a number of angiogenic factors, including CSPG4 [30,46], ANGPT2 [32,47] and MMPs [48,49]; as well as osteogenic factors such as S100A10 [37,50], osteolectin (CLEC11A) [34], together with BMP [51] and FGF related proteins [52,53]. In addition, the GP will contain some mineralized cartilage, and residual mineral within the GP ECM derived scaffolds may also contribute to its osteo-inductivity [11]. In contrast to the GP, AC ECM derived scaffolds supported the development of a hyaline-like cartilaginous tissue. This can be attributed to the fact that the AC ECM is rich in type II collagen, which is known to be chondro-inductive [54], and the presence of hypertrophic inhibitors and cartilage homeostasis regulators such as GREM1 [39,55] and TGFβi/βIGH3 [40,41]. For instance, GREM1 is a highly conserved glycoprotein known to function as a BMP antagonist. GREM1 predominantly regulates BMP2, 4 and 7, and plays an essential role in normal progression of limb bud patterning development [55,56]. TGFβi is a protein induced by TGFβ and is believed to have an effect in the early stages of cartilage development by promoting the adhesion and growth of pre-chondrogenic cells, but negatively regulates mineralization during the terminal stages of chondrogenic differentiation [57]. Previous mass spectrometry studies of AC have also revealed the presence of these proteins at different depths in human articular cartilage and other cartilaginous tissues [58,59]. Our work builds on these previous studies, and when combined with the detailed mass spectrometry analysis of other tissue specific ECMs [26,60], provides an understanding for how the unique

composition of GP and AC might make them particularly suitable as base biomaterials for bone and articular cartilage repair, respectively.

Following a detailed analysis demonstrating the capacity of these bi-layered ECM derived scaffolds to support spatially defined stem cell differentiation *in vitro*, they were next compared to a market-leading scaffold (Maioregen) [61] for their capacity to promote osteochondral defect regeneration *in vivo*. This nano-composite multi-layered biomaterial has previously been shown to promote improved osteochondral defect regeneration compared to empty controls [62]. Healing of the osseous region of the OC defects appeared to occur via different mechanisms when comparing the control scaffold and experimental AC-GP ECM scaffolds. Following implantation of the AC-GP ECM derived scaffold, evidence of remnant cartilage tissue within the osseous phase of the defect was detected at 6 months, which appeared to be replaced by fully-integrated, mature bone at month 12. This suggests that bone regeneration was occurring, at least in part, by endochondral ossification. In contrast, the control scaffold appeared to elicit bone regeneration primarily via the intramembranous pathway, as minimal intermediary cartilage tissue was detected within the osseous region at either time point. This may be due to the composition of the control scaffold, specifically the magnesium enriched hydroxyapatite (Mg-HA) and collagen type I, which have been shown to induce direct ossification [63]. Interestingly, implantation of either scaffold resulted in similar levels of bone healing by 12 months. Development of such a well-integrated, stable subchondral bone plate is thought to be vital to facilitate and maintain an upper layer of healthy repair cartilage.

Six months after implantation, higher levels of cartilage tissue were detected in the chondral region of defects treated with the experimental ECM scaffold. Furthermore, the collagen network within the repair cartilage that formed following implantation of AC-GP scaffolds better mimicked the zonal architecture characteristic of native articular cartilage. Development of an organized collagen fiber network is critical to support normal load bearing and extend

the protective function of cartilage [64], potentially leading to superior long-term outcomes compared to that achieved when a more disorganized, fibro-cartilage repair tissue forms. It is tempting to speculate that the development of such an organized cartilage repair tissue is, at least in part, related to the underlying bone regenerating via endochondral ossification. During normal joint development, the cartilage functions as a surface growth plate prior to skeletal maturity [65], with zonally organized articular cartilage only emerging at skeletal maturity [64]. Therefore, the AC-GP scaffolds may be recapitulating aspects of normal joint development by promoting articular cartilage formation over a layer of transient cartilage that is undergoing endochondral ossification.

Porcine ECM is commonly used in the development of scaffolds used clinically for soft tissue repair, however, successful clinical translation of xenogeneic tissue-derived ECM scaffolds requires efficient decellularization of the tissue to prevent an adverse immune response [66]. While the AC-GP scaffolds did not appear to elicit any negative immune response *in vitro* or *in vivo*, further studies will be required to validate this prior to clinical translation in human. Furthermore, if more extensive decellularization protocols are deemed necessary, further mass spectrometry analysis will be required to establish how such chemical treatments influence the composition of the resulting scaffold. Additionally, comparative analysis to the composition of other ECM derived bioscaffolds (e.g. small intestinal submucosa) is warranted to further support the need for tissue-specific ECM derived scaffolds for the regeneration of complex tissues. There are some other limitations with the proposed strategy for joint regeneration. While both scaffolds promoted hyaline cartilage tissue formation, it should be noted that this was not consistently attained in either group, with some animal-to-animal variability observed. This points to the need for improvements in the design of such ECM-based biomaterials targeting the musculoskeletal system. Strategies worthy of investigation include actively directing orientation of cell-deposited tissue by incorporating scaffolds with anisotropic

microarchitecture [67,68] and functionalization of the scaffolds with growth factors known to play major roles in supporting hyaline cartilage formation.

5. Conclusion

Taken together, these results demonstrate the value of using tissue-specific ECM to support regeneration of complex tissues such as the osteochondral unit. Biological scaffolds derived from the ECM of small intestinal submucosa (SIS) and other tissues have paved the way for clinical application, with widespread success achieved in several reconstructive surgical-procedures such as skin replacement, vascular grafts and skeletal muscle regeneration [69]. We propose that the use of layered, tissue-specific ECM derived scaffolds, designed with the end application in mind, would build upon this early success and lead to the successful, long-term repair of complex tissues.

Data availability

The authors declare that all data supporting the findings of this study are available within the paper and its Supplementary Information.

Appendix A. Supplementary data

See the section after *References*. Supplementary data to this article can be also found online at: https://doi.org/10.1016/j.biomaterials.2018.09.044.

Competing interests

The authors have no competing interests to declare.

Acknowledgements

Funding for this study was provided by the European Research Council Starter Grant (StemRepair – Project number: 258463), Science Foundation Ireland (SFI/12/RC/2278; 12/IA/1554), Enterprise Ireland (CF/2014/4325) and the Irish Research Council (GOIPG/2015/3186). The authors would like to thank: Dr. Kieran Wynne (Proteome Research Centre, Conway Institute of Biomolecular and Biomedical Research, University College Dublin, mass spectrometry), anesthesia and surgery personnel (University College Dublin) and the Centre for Research on Adaptive Nanostructures and Nanodevices (CRANN, Scanning Electron Microscopy).

References

[1] T.W. Gilbert, T.L. Sellaro, S.F. Badylak, Decellularization of tissues and organs, Biomaterials. 27 (2006) 3675–3683. doi:10.1016/j.biomaterials.2006.02.014.

[2] K.E.M. Benders, P.R. van Weeren, S.F. Badylak, D.B.F. Saris, W.J.A. Dhert, J. Malda, Extracellular matrix scaffolds for cartilage and bone regeneration, Trends Biotechnol. 31 (2013) 169–176. doi:10.1016/j.tibtech.2012.12.004.

[3] S.F. Badylak, Xenogeneic extracellular matrix as a scaffold for tissue reconstruction, Transpl. Immunol. 12 (2004) 367–377. doi:10.1016/j.trim.2003.12.016.

[4] C. Frantz, K.M. Stewart, V.M. Weaver, The extracellular matrix at a glance, J. Cell Sci. 123 (2010) 4195–4200. doi:10.1242/jcs.023820.

[5] B.N. Brown, S.F. Badylak, Extracellular Matrix as an Inductive Scaffold for Functional Tissue Reconstruction, Transl. Regen. Med. to Clin. 163 (2015) 11–29. doi:10.1016/B978-0-12-800548-4.00002-4.

[6] J.L. Dziki, L. Huleihel, M.E. Scarritt, S.F. Badylak, Extracellular Matrix Bioscaffolds as Immunomodulatory Biomaterials, Tissue Eng. Part A. 23 (2017) 1152–1159. doi:10.1089/ten.tea.2016.0538.

[7] L. Huleihel, J.L. Dziki, J.G. Bartolacci, T. Rausch, M.E. Scarritt, M.C. Cramer, T. Vorobyov, S.T. LoPresti, I.T. Swineheart, L.J. White, B.N. Brown, S.F. Badylak, Macrophage phenotype in response to ECM bioscaffolds, Semin. Immunol. 29 (2017) 2–13. doi:10.1016/j.smim.2017.04.004.

[8] S.F. Badylak, The extracellular matrix as a biologic scaffold material, Biomaterials. 28 (2007) 3587–93. doi:10.1016/j.biomaterials.2007.04.043.

[9] H. V Almeida, G.M. Cunniffe, T. Vinardell, C.T. Buckley, F.J. O'Brien, D.J. Kelly, Coupling freshly isolated CD44(+) infrapatellar fat pad-derived stromal cells with a TGF-β3 eluting cartilage ECM-derived scaffold as a single-stage strategy for promoting chondrogenesis, Adv. Healthc. Mater. 4 (2015) 1043–53. doi:10.1002/adhm.201400687.

[10] K. Shimomura, B.B. Rothrauff, R.S. Tuan, Region-Specific Effect of the Decellularized Meniscus Extracellular Matrix on Mesenchymal Stem Cell–Based Meniscus Tissue Engineering, Am. J. Sports Med. 45 (2017) 604–611. doi:10.1177/0363546516674184.

[11] G.M. Cunniffe, P.J. Díaz-Payno, J.S. Ramey, O.R. Mahon, A. Dunne, E.M. Thompson, F.J. O'Brien, D.J. Kelly, Growth plate extracellular matrix-derived scaffolds for large bone defect healing, Eur. Cell. Mater. 33 (2017) 130–142. doi:10.22203/eCM.v033a10.

[12] F. Gao, Z. Xu, Q. Liang, B. Liu, H. Li, Y. Wu, Y. Zhang, Z. Lin, M. Wu, C. Ruan, W. Liu, Direct 3D Printing of High Strength Biohybrid Gradient Hydrogel Scaffolds for Efficient Repair of Osteochondral Defect, Adv. Funct. Mater. 28 (2018) 1706644. doi:10.1002/adfm.201706644.

[13] Y. Wu, S. Zhu, C. Wu, P. Lu, C. Hu, S. Xiong, J. Chang, B.C. Heng, Y. Xiao, H.W. Ouyang, A Bi-Lineage Conducive Scaffold for Osteochondral Defect Regeneration, Adv. Funct. Mater. 24 (2014) 4473–4483. doi:10.1002/adfm.201304304.

[14] T.J. Levingstone, A. Ramesh, R.T. Brady, P.A.J. Brama, C. Kearney, J.P. Gleeson, F.J. O'Brien, Cell-free multi-layered collagen-based scaffolds demonstrate layer specific regeneration of functional osteochondral tissue in caprine joints, Biomaterials. 87 (2016) 69–81. doi:10.1016/j.biomaterials.2016.02.006.

[15] S.N. Dehghani, A.S. Bigham, S. Torabi Nezhad, Z. Shafiei, Effect of bovine fetal growth plate as a new xenograft in experimental bone defect healing: radiological, histopathological and biomechanical evaluation, Cell Tissue Bank. 9 (2008) 91–99. doi:10.1007/s10561-008-9062-7.

[16] A.S. Bigham, S.N. Dehghani, Z. Shafiei, S.T. Nezhad, Experimental bone defect healing with xenogenic demineralized bone matrix and bovine fetal growth plate as a new xenograft: radiological, histopathological and biomechanical evaluation, Cell Tissue Bank. 10 (2009) 33–41. doi:10.1007/s10561-008-9107-y.

[17] A. Bigham-Sadegh, I. Karimi, A. Oryan, E. Mahmoudi, Z. Shafiei-Sarvestani, Spinal fusion with demineralized calf fetal growth plate as novel biomaterial in rat model: a preliminary study, Int. J. Spine Surg. 8 (2014) 5–5. doi:10.14444/1005.

[18] H. V. Almeida, R. Eswaramoorthy, G.M. Cunniffe, C.T. Buckley, F.J. O'Brien, D.J. Kelly, Fibrin hydrogels functionalized with cartilage extracellular matrix and incorporating freshly isolated stromal cells as an injectable for cartilage regeneration, Acta Biomater. 36 (2016) 55–62. doi:10.1016/j.actbio.2016.03.008.

[19] Z. Yang, Y. Shi, X. Wei, J. He, S. Yang, G. Dickson, J. Tang, J. Xiang, C. Song, G. Li, Fabrication and repair of cartilage defects with a novel acellular cartilage matrix scaffold, Tissue Eng. Part C Methods. 16 (2010) 865–76. doi:10.1089/ten.TEC.2009.0444.

[20] H. V. Almeida, Y. Liu, G.M. Cunniffe, K.J. Mulhall, A. Matsiko, C.T. Buckley, F.J. O'Brien, D.J. Kelly, Controlled release of transforming growth factor-β3 from cartilage-extra-cellular-matrix-derived scaffolds to promote chondrogenesis of human-joint-tissue-derived stem cells, Acta Biomater. 10 (2014) 4400–9. doi:10.1016/j.actbio.2014.05.030.

[21] X. Jiang, M. Ye, X. Jiang, G. Liu, S. Feng, L. Cui, H. Zou, Method Development of Efficient Protein Extraction in Bone Tissue for Proteome Analysis research articles, J. Proteome Res. 6 (2007) 2287–2294.

[22] T. Zhou, C. Li, W. Zhao, X. Wang, F. Wang, J. Sha, MaxReport: An Enhanced Proteomic Result Reporting Tool for MaxQuant., PLoS One. 11 (2016) e0152067. doi:10.1371/journal.pone.0152067.

[23] S. Tyanova, T. Temu, J. Cox, The MaxQuant computational platform for mass spectrometry-based shotgun proteomics., Nat. Protoc. 11 (2016) 2301–2319. doi:10.1038/nprot.2016.136.

[24] J. Cox, I. Matic, M. Hilger, N. Nagaraj, M. Selbach, J. V Olsen, M. Mann, A practical guide to the MaxQuant computational platform for SILAC-based quantitative proteomics., Nat. Protoc. 4 (2009) 698–705. doi:10.1038/nprot.2009.36.

[25] S. Tyanova, T. Temu, P. Sinitcyn, A. Carlson, M.Y. Hein, T. Geiger, M. Mann, J. Cox, The Perseus computational platform for comprehensive analysis of (prote)omics data, Nat. Methods. 13 (2016) 731–740. doi:10.1038/nmeth.3901.

[26] A. Naba, K.R. Clauser, H. Ding, C.A. Whittaker, S.A. Carr, R.O. Hynes, The extracellular matrix: Tools and insights for the "omics" era, Matrix Biol. 49 (2016)

10–24. doi:10.1016/j.matbio.2015.06.003.

[27] N.Y. Ignat'eva, N.A. Danilov, S. V. Averkiev, M. V. Obrezkova, V. V. Lunin, E.N. Sobol', Determination of hydroxyproline in tissues and the evaluation of the collagen content of the tissues, J. Anal. Chem. 62 (2007) 51–57. doi:10.1134/S106193480701011X.

[28] P. Mainil-Varlet, B. Van Damme, D. Nesic, G. Knutsen, R. Kandel, S. Roberts, A new histology scoring system for the assessment of the quality of human cartilage repair: ICRS II, Am. J. Sports Med. 38 (2010) 880–890. doi:10.1177/0363546509359068.

[29] N. Reznikov, R. Almany-Magal, R. Shahar, S. Weiner, Three-dimensional imaging of collagen fibril organization in rat circumferential lamellar bone using a dual beam electron microscope reveals ordered and disordered sub-lamellar structures, Bone. 52 (2013) 676–683. doi:10.1016/j.bone.2012.10.034.

[30] J. Fukushi, I.T. Makagiansar, W.B. Stallcup, NG2 proteoglycan promotes endothelial cell motility and angiogenesis via engagement of galectin-3 and alpha3beta1 integrin., Mol. Biol. Cell. 15 (2004) 3580–90. doi:10.1091/mbc.E04-03-0236.

[31] U. Ozerdem, W.B. Stallcup, Pathological angiogenesis is reduced by targeting pericytes via the NG2 proteoglycan, Angiogenesis. 7 (2004) 269–276. doi:10.1007/s10456-004-4182-6.

[32] T. Kadomatsu, M. Endo, K. Miyata, Y. Oike, Diverse roles of ANGPTL2 in physiology and pathophysiology, Trends Endocrinol. Metab. 25 (2014) 245–254. doi:10.1016/j.tem.2014.03.012.

[33] Y. Kubota, Unveiling Angptl2, a rising HSC expander, Blood. 124 (2014) 833–834. doi:10.1182/blood-2014-06-581629.

[34] R. Yue, B. Shen, S.J. Morrison, Clec11a/osteolectin is an osteogenic growth factor that promotes the maintenance of the adult skeleton, Elife. 5 (2016) 27. doi:10.7554/eLife.18782.

[35] M. Inada, Y. Wang, M.H. Byrne, M.U. Rahman, C. Miyaura, C. Lopez-Otin, S.M. Krane, Critical roles for collagenase-3 (Mmp13) in development of growth plate cartilage and in endochondral ossification, Proc. Natl. Acad. Sci. 101 (2004) 17192–17197. doi:10.1073/pnas.0407788101.

[36] D. Stickens, Altered endochondral bone development in matrix metalloproteinase 13-deficient mice, Development. 131 (2004) 5883–5895. doi:10.1242/dev.01461.

[37] A. Cmoch, A. Strzelecka-Kiliszek, M. Palczewska, P. Groves, S. Pikula, S100A4 and S100A10 proteins as regulators of matrix vesicle mediated mineralization of osteoblast-like cells, Bone. 50 (2012) S69–S70. doi:10.1016/j.bone.2012.02.196.

[38] R. Donato, B. R. Cannon, G. Sorci, F. Riuzzi, K. Hsu, D. J. Weber, C. L. Geczy,

Functions of S100 Proteins, Curr. Mol. Med. 13 (2013) 24–57. doi:10.2174/156652413804486214.

[39] J.C.H. Leijten, J. Emons, C. Sticht, S. Van Gool, E. Decker, A. Uitterlinden, G. Rappold, A. Hofman, F. Rivadeneira, S. Scherjon, J.M. Wit, J. Van Meurs, C.A. Van Blitterswijk, M. Karperien, Gremlin 1, frizzled-related protein, and dkk-1 are key regulators of human articular cartilage homeostasis, Arthritis Rheum. 64 (2012) 3302–3312. doi:10.1002/art.34535.

[40] S. Ohno, T. Doi, S. Tsutsumi, Y. Okada, K. Yoneno, Y. Kato, K. Tanne, RGD-CAP (βig-h3) is expressed in precartilage condensation and in prehypertrophic chondrocytes during cartilage development, Biochim. Biophys. Acta - Gen. Subj. 1572 (2002) 114–122. doi:10.1016/S0304-4165(02)00286-6.

[41] S. Ohno, M. Noshiro, S. Makihira, T. Kawamoto, M. Shen, W. Yan, Y. Kawashima-Ohya, K. Fujimoto, K. Tanne, Y. Kato, RGD-CAP (βig-h3) enhances the spreading of chondrocytes and fibroblasts via integrin α1β1, Biochim. Biophys. Acta - Mol. Cell Res. 1451 (1999) 196–205. doi:10.1016/S0167-4889(99)00093-2.

[42] M.S. Bendre, D.C. Montague, T. Peery, N.S. Akel, D. Gaddy, L.J. Suva, Interleukin-8 stimulation of osteoclastogenesis and bone resorption is a mechanism for the increased osteolysis of metastatic bone disease, Bone. 33 (2003) 28–37. doi:10.1016/S8756-3282(03)00086-3.

[43] P. Kopesky, K. Tiedemann, D. Alkekhia, C. Zechner, B. Millard, B. Schoeberl, S. V. Komarova, Autocrine signaling is a key regulatory element during osteoclastogenesis, Biol. Open. 3 (2014) 767–776. doi:10.1242/bio.20148128.

[44] A.M. Handorf, W.-J. Li, Fibroblast Growth Factor-2 Primes Human Mesenchymal Stem Cells for Enhanced Chondrogenesis, PLoS One. 6 (2011) e22887. doi:10.1371/journal.pone.0022887.

[45] E. Kon, G. Filardo, F. Perdisa, G. Venieri, M. Marcacci, Clinical results of multilayered biomaterials for osteochondral regeneration, J. Exp. Orthop. 1 (2014) 10. doi:10.1186/s40634-014-0010-0.

[46] J.I. Fukushi, M. Inatani, Y. Yamaguchi, W.B. Stallcup, Expression of NG2 proteoglycan during endochondral and intramembranous ossification, Dev. Dyn. 228 (2003) 143–148. doi:10.1002/dvdy.10359.

[47] W. De Spiegelaere, P. Cornillie, C. Casteleyn, C. Burvenich, W. Van den Broeck, Detection of Hypoxia Inducible Factors and Angiogenic Growth Factors during Foetal Endochondral and Intramembranous Ossification, J. Vet. Med. Ser. C Anat. Histol. Embryol. 39 (2010) 376–384. doi:10.1111/j.1439-0264.2010.01005.x.

[48] T.H. Vu, J.M. Shipley, G. Bergers, J.E. Berger, J.A. Helms, D. Hanahan, S.D. Shapiro, R.M. Senior, Z. Werb, MMP-9/gelatinase B is a key regulator of growth plate

angiogenesis and apoptosis of hypetrophic chondrocytes, Cell. 93 (1998) 411–422. doi:10.1016/S0092-8674(00)81169-1.

[49] H. Nagai, M. Aoki, Inhibition of growth plate angiogenesis and endochondral ossification with diminished expression of MMP-13 in hypertrophic chondrocytes in FGF-2-treated rats, J. Bone Miner. Metab. 20 (2002) 142–147. doi:10.1007/s007740200020.

[50] L.L. Lourido, V. Calamia, J.J. Mateos, P. Fernandez-Puente, J. Fernandez-Tajes, F.J. Blanco, C. Ruiz-Romero, P. Fernández-Puente, J. Fernández-Tajes, F.J. Blanco, C. Ruiz-Romero, Quantitative proteomic profiling of human articular cartilage degradation in osteoarthritis., J. Proteome Res. 13 (2014) 6096–106. doi:10.1021/pr501024p.

[51] H.C. Anderson, P.T. Hodges, X.M. Aguilera, L. Missana, P.E. Moylan, Bone Morphogenetic Protein (BMP) Localization in Developing Human and Rat Growth Plate, Metaphysis, Epiphysis, and Articular Cartilage, J. Histochem. Cytochem. 48 (2000) 1493–1502. doi:10.1177/002215540004801106.

[52] E. Tchetina, F. Mwale, a R. Poole, Distinct phases of coordinated early and late gene expression in growth plate chondrocytes in relationship to cell proliferation, matrix assembly, remodeling, and cell differentiation., J. Bone Miner. Res. 18 (2003) 844–51. doi:10.1359/jbmr.2003.18.5.844.

[53] A.I. Alford, K.M. Kozloff, K.D. Hankenson, Extracellular matrix networks in bone remodeling, Int. J. Biochem. Cell Biol. 65 (2015) 20–31. doi:10.1016/j.biocel.2015.05.008.

[54] M. Tamaddon, M. Burrows, S.A. Ferreira, F. Dazzi, J.F. Apperley, A. Bradshaw, D.D. Brand, J. Czernuszka, E. Gentleman, Monomeric, porous type II collagen scaffolds promote chondrogenic differentiation of human bone marrow mesenchymal stem cells in vitro, Sci. Rep. 7 (2017) 1–10. doi:10.1038/srep43519.

[55] M.K. Khokha, D. Hsu, L.J. Brunet, M.S. Dionne, R.M. Harland, Gremlin is the BMP antagonist required for maintenance of Shh and Fgf signals during limb patterning, Nat. Genet. 34 (2003) 303–307. doi:10.1038/ng1178.

[56] D.L. Worthley, M. Churchill, J.T. Compton, Y. Tailor, M. Rao, Y. Si, D. Levin, M.G. Schwartz, A. Uygur, Y. Hayakawa, S. Gross, B.W. Renz, W. Setlik, A.N. Martinez, X. Chen, S. Nizami, H.G. Lee, H.P. Kang, J.-M. Caldwell, S. Asfaha, C.B. Westphalen, T. Graham, G. Jin, K. Nagar, H. Wang, M.A. Kheirbek, A. Kolhe, J. Carpenter, M. Glaire, A. Nair, S. Renders, N. Manieri, S. Muthupalani, J.G. Fox, M. Reichert, A.S. Giraud, R.F. Schwabe, J.-P. Pradere, K. Walton, A. Prakash, D. Gumucio, A.K. Rustgi, T.S. Stappenbeck, R.A. Friedman, M.D. Gershon, P. Sims, T. Grikscheit, F.Y. Lee, G. Karsenty, S. Mukherjee, T.C. Wang, Gremlin 1 identifies a skeletal stem cell with bone, cartilage and reticular stromal potential, Cell. 160 (2015) 269–84. doi:10.1016/j.cell.2014.11.042.

[57] N. Thapa, B.H. Lee, I.S. Kim, TGFBIp/βig-h3 protein: A versatile matrix molecule induced by TGF-β, Int. J. Biochem. Cell Biol. 39 (2007) 2183–2194. doi:10.1016/j.biocel.2007.06.004.

[58] P. Önnerfjord, A. Khabut, F.P. Reinholt, O. Svensson, D. Heinegård, Quantitative proteomic analysis of eight cartilaginous tissues reveals characteristic differences as well as similarities between subgroups, J. Biol. Chem. 287 (2012) 18913–24. doi:10.1074/jbc.M111.298968.

[59] M.F. Hsueh, A. Khabut, S. Kjellström, P. Önnerfjord, V.B. Kraus, Elucidating the Molecular Composition of Cartilage by Proteomics, J. Proteome Res. 15 (2016) 374–388. doi:10.1021/acs.jproteome.5b00946.

[60] A. Naba, O.M.T. Pearce, A. Del Rosario, D. Ma, H. Ding, V. Rajeeve, P.R. Cutillas, F.R. Balkwill, R.O. Hynes, Characterization of the Extracellular Matrix of Normal and Diseased Tissues Using Proteomics, J. Proteome Res. 16 (2017) 3083–3091. doi:10.1021/acs.jproteome.7b00191.

[61] M. Berruto, M. Delcogliano, F. de Caro, G. Carimati, F. Uboldi, P. Ferrua, G. Ziveri, C.F. De Biase, Treatment of Large Knee Osteochondral Lesions With a Biomimetic Scaffold: Results of a Multicenter Study of 49 Patients at 2-Year Follow-up, Am. J. Sports Med. 42 (2014) 1607–17. doi:10.1177/0363546514530292.

[62] E. Kon, M. Delcogliano, G. Filardo, M. Fini, G. Giavaresi, S. Francioli, I. Martin, D. Pressato, E. Arcangeli, R. Quarto, M. Sandri, M. Marcacci, Orderly osteochondral regeneration in a sheep model using a novel nano-composite multilayered biomaterial, J. Orthop. Res. 28 (2010) 116–124. doi:10.1002/jor.20958.

[63] G. Calabrese, R. Giuffrida, S. Forte, L. Salvatorelli, C. Fabbi, E. Figallo, M. Gulisano, R. Parenti, G. Magro, C. Colarossi, L. Memeo, R. Gulino, Bone augmentation after ectopic implantation of a cell-free collagen-hydroxyapatite scaffold in the mouse, Sci. Rep. 6 (2016) 1–10. doi:10.1038/srep36399.

[64] A.R. Gannon, T. Nagel, A.P. Bell, N.C. Avery, D.J. Kelly, Postnatal changes to the mechanical properties of articular cartilage are driven by the evolution of its Collagen network, Eur. Cells Mater. 29 (2015) 105–123. doi:vol029a09 [pii].

[65] H.M. Kronenberg, H.M. Kronenberg, Developmental regulation of the growth plate, Nature. 423 (2003) 332–6. doi:10.1038/nature01657.

[66] P.M. Crapo, T.W. Gilbert, S.F. Badylak, An overview of tissue and whole organ decellularization processes, Biomaterials. 32 (2011) 3233–43. doi:10.1016/j.biomaterials.2011.01.057.

[67] E.L.W. De Mulder, G. Hannink, T.H. Van Kuppevelt, W.F. Daamen, P. Buma, Similar Hyaline-Like Cartilage Repair of Osteochondral and Anisotropic Collagen Scaffolds, Tissue Eng. Part A. 20 (2014) 635–645. doi:10.1089/ten.tea.2013.0083.

[68] H. V. Almeida, B.N. Sathy, I. Dudurych, C.T. Buckley, F.J. O'Brien, D.J. Kelly, Anisotropic Shape-Memory Alginate Scaffolds Functionalized with Either Type I or Type II Collagen for Cartilage Tissue Engineering, Tissue Eng. Part A. 23 (2017) 55–68. doi:10.1089/ten.tea.2016.0055.

[69] B. Andrée, A. Bär, A. Haverich, A. Hilfiker, Small Intestinal Submucosa Segments as Matrix for Tissue Engineering: Review, Tissue Eng. Part B Rev. 19 (2013) 279–291. doi:10.1089/ten.teb.2012.0583.

Supporting Information

Appendix A. Supplementary data

Supplementary data to this article can be also found online at: https://doi.org/10.1016/j.biomaterials.2018.09.044.

Tissue-Specific Extracellular Matrix Scaffolds for the Regeneration of Spatially Complex Musculoskeletal Tissues

Gráinne M. Cunniffe[1], Pedro J. Díaz-Payno[1], Eamon J. Sheehy, Susan E. Critchley, Henrique V. Almeida, Pierluca Pitacco, Simon F. Carroll, Olwyn R. Mahon; Aisling Dunne, Tanya J. Levingstone, Conor J. Moran, Robert T. Brady, Fergal J. O'Brien, Pieter A.J. Brama, Daniel J. Kelly*

[1] The authors made equal contribution to the work.

*Corresponding author: Prof. D. J. Kelly. Trinity College Dublin, Ireland. E-mail: kellyd9@tcd.ie

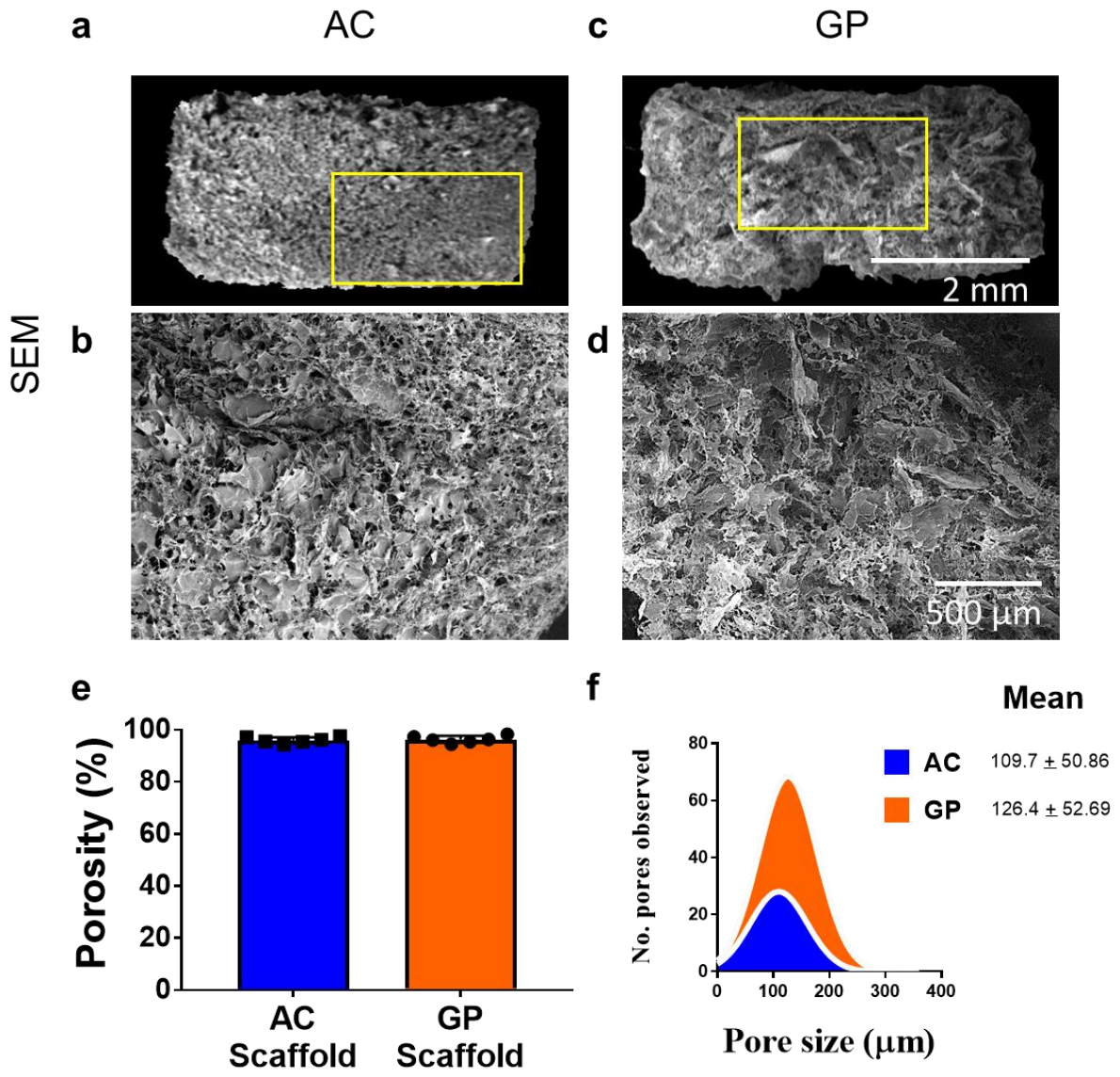

Fig. S1. Characterization of porosity and pore size of AC and GP ECM derived scaffolds. a-b) SEM of AC ECM scaffolds at different magnifications. c-d) SEM of GP ECM scaffolds at different magnifications. e) porosity of AC and GP scaffolds [porosity = 1-(dw/(V*δH_2O))]. f) Pore size of each scaffold based on SEM images ($n \geq 3$), calculated with Image J.

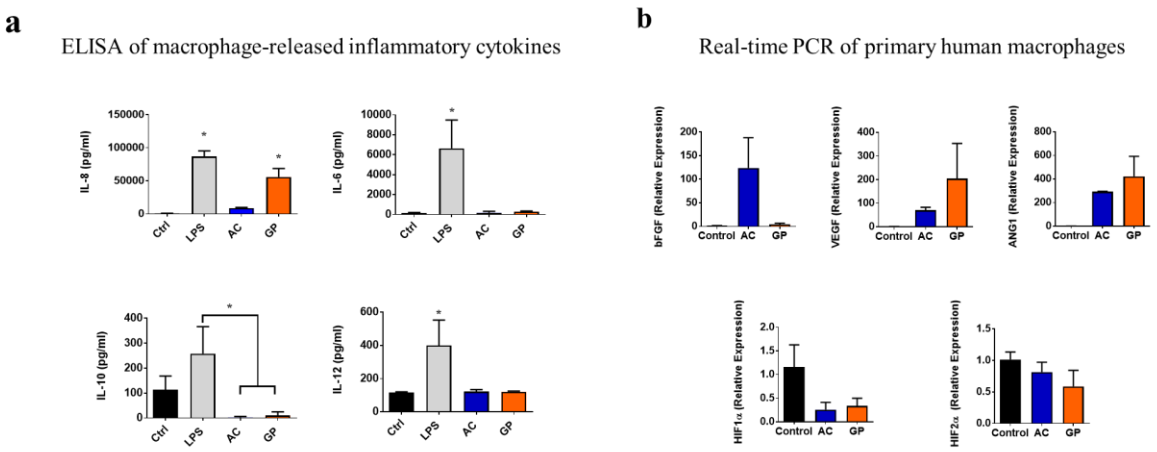

Fig. S2. Evaluation of scaffold-induced cytokine production and gene expression in primary human macrophages. a) Inflammatory cytokine production by macrophages was evaluated following contact with AC and GP ECM tissues after 7 days. Cell supernatants were assessed for IL-8, IL-6, IL-10 and IL-12 by ELISA. LPS was included as a positive control and untreated macrophages as a negative control. b) Real-time PCR, carried out on primary human macrophages cultured in the presence of scaffold material, highlights a trend towards differential expression of key soluble factors (bFGF, VEGF, Ang1) and hypoxia-inducible transcription factors, modulators of tissue repair. Results shown are means (± SD) and are representative of 3 independent experiments. *$p \leq 0.05$.

Table S1. Scoring System Assessment Criteria (adapted from ICRS II system)

Histological Parameter Details	Grading	Score
a. Tissue Morphology Evaluated using safranin O and polarised light microscopy of picrosirius red staining	Collagen fibres detectable, oriented parallel to the surface in the superficial zone and vertical in the deep zone.	100
	Fibrocartilage with collagen fibres and blood vessels	0
b. Matrix Staining It can be assessed using safranin O or toluidine blue.	Strong full thickness staining (full metachromasia).	100
	Absence of staining	0
c. Cell Morphology	Mostly rounded/oval cells. Presence of peri-cellular lacuna	100
	More elongated/spindle-shaped cells. Less rounded/oval cells	0
d. Chondrocyte Clustering A chondrocyte cluster is defined as a group of at least 4 cells. Considered a negative feature.	Absence	100
	Presence	0
e. Surface Architecture	Smooth	100
	Delaminated, disrupted	0
f. Formation of a Tidemark	Presence of a tidemark along the whole surface	100
	Lack of visible interface	0
g. Subchondral Bone Abnormalities	Absence of abnormality	100
	Subchondral interface characterised by either fracture, sclerosis, disruption, or intense remodelling, with or without fibrovascular infiltration into the marrow. Marrow fibrosis	0
h. Abnormal calcification/ossification	Absence of extensive ossification	100
	Presence of extensive ossification	0
Criteria (i-m) below address more overall assessments, assimilating several/all of the parameters listed above.		

i. Surface/Superficial Assessment The evaluation should be performed on the upper third of the cartilage tissue	Intact surface with elongated cells and collagen fibres parallel to the surface in the most superficial zone.	100
	A severally disrupted surface with no obvious fibre organisation.	0
j. Mid/deep zone assessment The lower two thirds of the tissue should be evaluated in this parameter	Area rich in proteoglycans, with detectable fibres closer to the deep zone.	100
	Absence of proteoglycans, detectable fibres between the upper and mid zone.	0
k. Overall Assessment This parameter requires the observer to generate an overall assessment of the quality of the repaired tissue	Hyaline articular cartilage	100
	Fibrous tissue	0
l. Average Combined Scores		100
		0
m. Average Cartilage Scores		100
		0

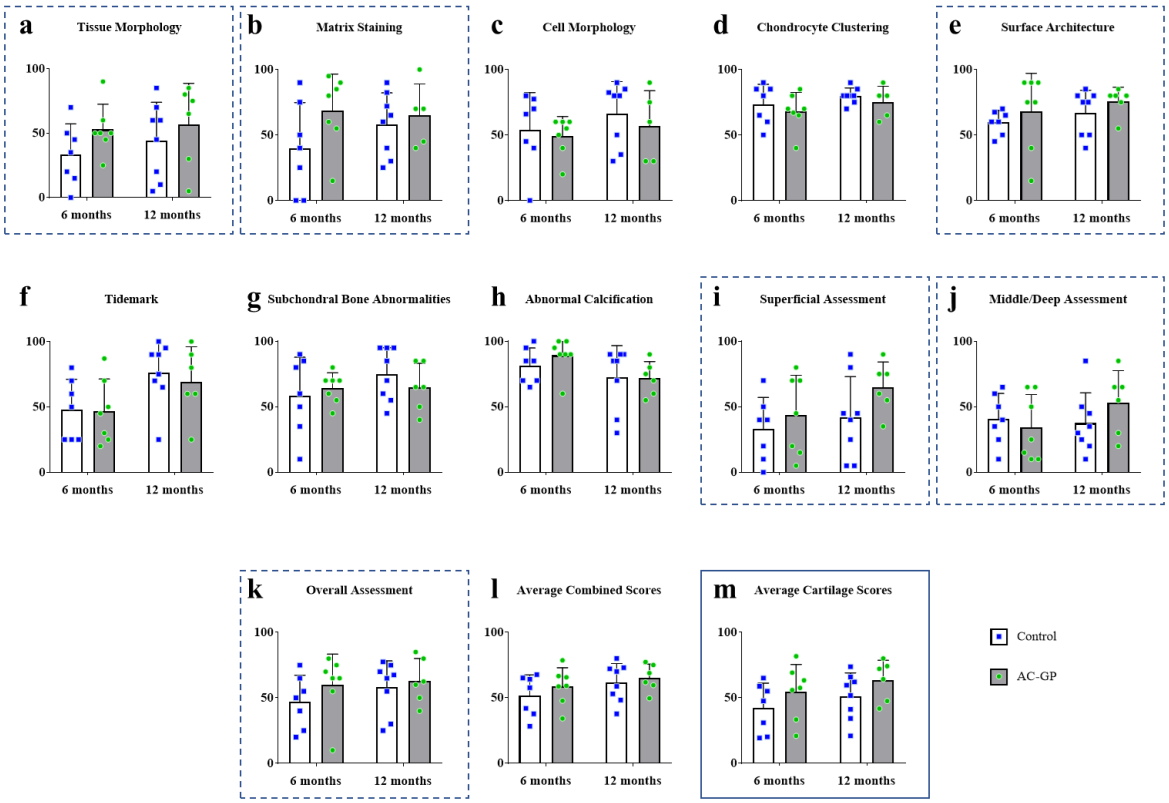

Fig. S3. ICRS scores for treated defects at 6 and 12 months. ICRS Scoring system was applied to histological samples for control and AC-GP treated groups at 6 and 12 months. No statistical differences were detected in any category. “Average Cartilage” score was defined as the ICRS scores related to the chondral region specifically, indicated by dashed squares, for control group 6 months: 42.32 ± 18.99, 12 months: 51.14 ± 17.82 and the AC-GP group 6 months: 54.52 ± 20.91, 12 months: 63.26 ± 15.44.

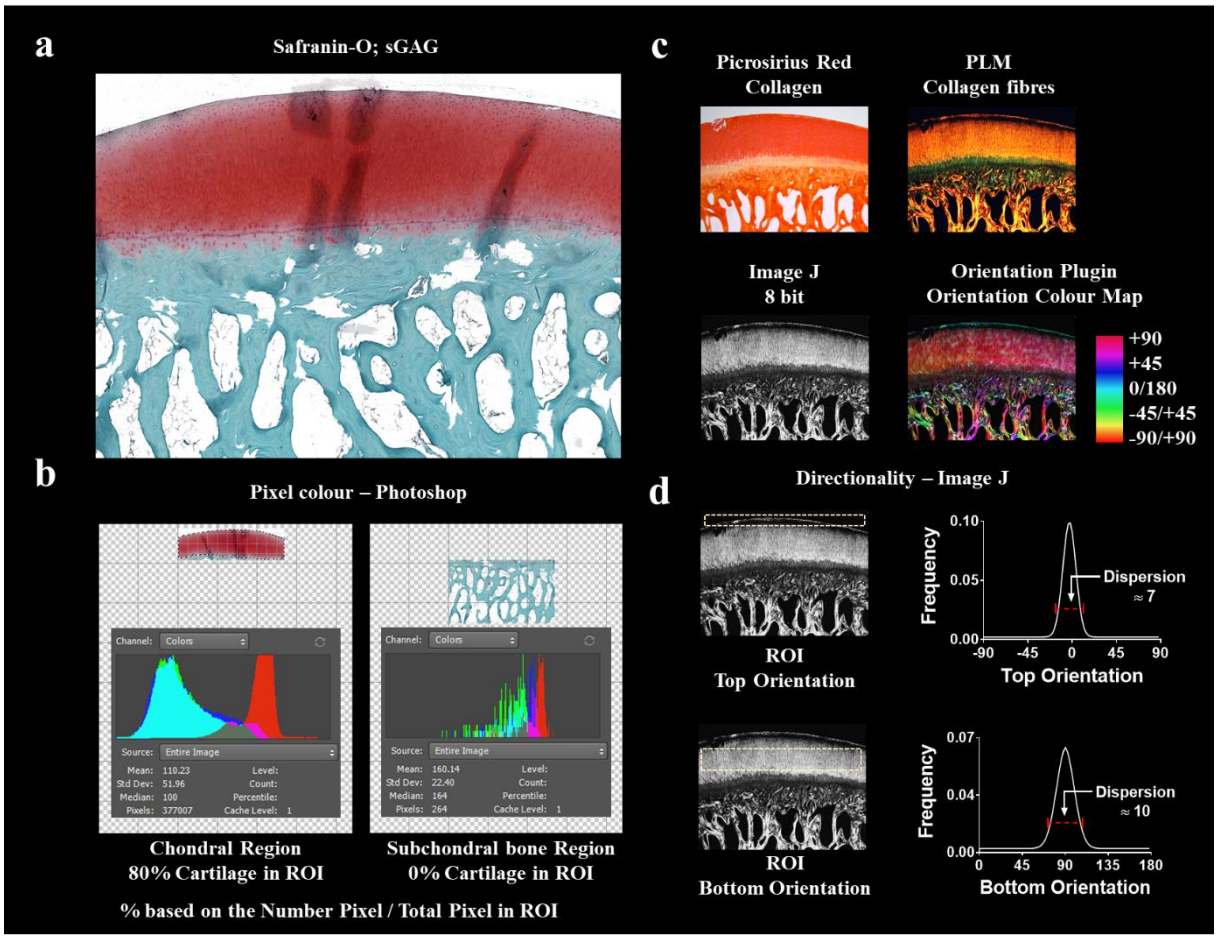

Fig. S4. Outline of the methodology used to assess % Cartilage in a specific region of interest (ROI) and the collagen fibre orientation within repair tissue. a) Histological image of an osteochondral plug with sulfated glycosaminoglycan (sGAG) stained red with Safranin-O. b) calculation of % cartilage based on the number of pixels with the average red color, divided by the total amount of pixels in the ROI, 1.5 mm x 5 mm for the chondral region (CR) and 3.5 x 5 mm for the subchondral bone region, just under the CR. c) Picrosirius red stained samples are imaged under polarized light microscopy (PLM) to view collagen fibres. d) Directionality analysis of the fibre orientation is quantified on the corresponding 8-bit images (color map is a validation example). Due to the curved surface of the joint, the minimum dispersion value of the fibres is 7. Orientation can be any value as it corresponds to the average of orientations among the fibres. Dispersion can be considered as a measurement of the quality of the orientation value, i.e. how similar the orientation of each fibre is to others within the sample.

Table S2. List of proteins detected in Articular Cartilage ECM using Mass Spectrometry

LFQ intensity AC_1	LFQ intensity AC_2	LFQ intensity AC_3	Peptides	Unique peptides	Score	Intensity	Gene name	Division Matrisome	Subcategory matrisome
28.35758	28.80888	NaN	15	14	191.17	20304000000	COL11A1	Core matrisome	Collagens
35.40952	34.97002	35.00299	39	38	323.31	2.3936E+11	COL11A2	Core matrisome	Collagens
33.9656	33.75663	34.17027	57	2	323.31	38906000000	COL14A1	Core matrisome	Collagens
30.21917	NaN	29.90455	56	1	11.516	2702800000	COL14A1	Core matrisome	Collagens
30.03131	30.51126	29.03215	8	3	80.797	9189500000	COL15A1	Core matrisome	Collagens
29.82595	31.0949	30.48884	4	4	31.884	10193000000	COL1A1	Core matrisome	Collagens
29.45621	29.78767	30.1966	13	13	93.924	20345000000	COL1A2	Core matrisome	Collagens
26.71882	NaN	27.05497	3	3	19.264	995870000	COL27A1	Core matrisome	Collagens
35.11644	34.73333	34.83295	17	16	323.31	2.6774E+11	COL2A1	Core matrisome	Collagens
32.60205	31.64212	32.57851	12	12	101.03	17787000000	COL6A1	Core matrisome	Collagens
30.19072	30.09093	29.33818	6	6	82.783	2976300000	COL6A1	Core matrisome	Collagens
31.58607	31.47315	31.90483	3	3	39.012	12479000000	COL6A1	Core matrisome	Collagens
33.7797	33.79333	33.70841	29	29	297.87	51108000000	COL6A2	Core matrisome	Collagens
34.93293	34.77254	34.54541	21	21	323.31	1.5189E+11	COL9A1	Core matrisome	Collagens
32.17435	32.00068	32.29655	5	5	82.195	48229000000	COL9A2	Core matrisome	Collagens
30.36953	29.97856	29.76819	9	9	59.91	6513200000	COL16A1	Core matrisome	Collagens
35.63591	35.75494	35.40616	122	122	323.31	1.7419E+11	COL6A3	Core matrisome	Collagens
29.61681	30.02789	28.93646	9	9	103.68	1982200000	AEBP1	Core matrisome	ECM Glycoproteins
27.90552	28.01324	NaN	12	12	77.517	519880000	CILP	Core matrisome	ECM Glycoproteins
33.22116	33.34982	33.67661	49	49	323.31	22944000000	CILP2	Core matrisome	ECM Glycoproteins
37.08738	36.81419	37.31697	41	13	323.31	5.5647E+11	COMP	Core matrisome	ECM Glycoproteins
29.53473	28.71158	NaN	30	2	96.405	2312400000	COMP	Core matrisome	ECM Glycoproteins
31.74523	32.44209	31.64757	6	6	67.35	19448000000	CTHRC1	Core matrisome	ECM Glycoproteins
31.56833	31.92447	31.66043	15	15	153.38	45634000000	EDIL3	Core matrisome	ECM Glycoproteins
28.52765	28.57762	28.0682	12	12	96.492	1429300000	EMILIN1	Core matrisome	ECM Glycoproteins
28.14957	28.08451	NaN	3	3	25.45	811680000	FBLN1	Core matrisome	ECM Glycoproteins
32.55472	32.94576	32.95489	17	17	136.14	21175000000	FBLN7	Core matrisome	ECM Glycoproteins
28.97544	28.8649	29.12943	9	9	58.825	1066200000	FBN1	Core matrisome	ECM Glycoproteins
24.79323	27.12898	26.11856	33	33	323.31	89384000000	FGB	Core matrisome	ECM Glycoproteins
34.73726	34.65874	34.67409	88	88	323.31	3.4305E+11	FN1	Core matrisome	ECM Glycoproteins
37.08074	36.47845	36.92702	39	39	323.31	2.962E+11	MATN1	Core matrisome	ECM Glycoproteins
30.20443	30.55938	29.762	12	12	117.15	10296000000	MATN2	Core matrisome	ECM Glycoproteins
37.14357	36.73568	37.05793	33	33	323.31	5.7601E+11	MATN3	Core matrisome	ECM Glycoproteins
33.79275	33.88231	33.8903	28	28	259.09	36329000000	MATN4	Core matrisome	ECM Glycoproteins
28.79359	28.05092	29.65901	3	3	22.131	1715400000	MFAP2	Core matrisome	ECM Glycoproteins
32.99988	32.80785	32.60373	24	24	274.88	60988000000	MFGE8	Core matrisome	ECM Glycoproteins
29.05876	28.1399	29.16065	8	8	79.437	1390000000	PCOLCE	Core matrisome	ECM Glycoproteins
28.63951	27.73731	NaN	8	8	61.368	1149700000	PCOLCE2	Core matrisome	ECM Glycoproteins
26.36785	NaN	26.58835	2	2	11.684	121600000	RSPO3	Core matrisome	ECM Glycoproteins
29.26578	29.26186	29.11642	4	4	31.414	1248200000	SMOC2	Core matrisome	ECM Glycoproteins
29.69515	29.70154	29.83711	9	9	79.112	17480000000	SPARC	Core matrisome	ECM Glycoproteins
29.57143	30.46314	29.03234	11	11	82.189	3741200000	SRPX	Core matrisome	ECM Glycoproteins
32.20557	31.93484	32.14643	23	23	197.48	9971900000	SRPX2	Core matrisome	ECM Glycoproteins
34.2187	34.00605	32.4233	28	28	289.22	33968000000	TGFBI	Core matrisome	ECM Glycoproteins

35.95359	35.83418	36.12303	62	61	323.31	3.0238E+11	THBS1	Core matrisome	ECM Glycoproteins
25.48195	26.16337	NaN	4	3	22.176	110530000	THBS2	Core matrisome	ECM Glycoproteins
30.387	31.02518	30.66043	18	16	130.19	22253000000	THBS3	Core matrisome	ECM Glycoproteins
30.37306	29.8798	30.4715	13	7	112.21	3060900000	THBS4	Core matrisome	ECM Glycoproteins
35.09926	34.73605	34.71416	64	18	323.31	80969000000	TNC	Core matrisome	ECM Glycoproteins
26.91866	NaN	27.15991	48	2	37.083	147120000	TNC	Core matrisome	ECM Glycoproteins
32.6145	33.06519	32.45405	22	22	323.31	20351000000	VIT	Core matrisome	ECM Glycoproteins
26.12056	26.68405	NaN	4	4	64.28	347450000	VWA1	Core matrisome	ECM Glycoproteins
27.12524	27.05703	NaN	21	21	306.7	75371000000	FGG	Core matrisome	ECM Glycoproteins
38.15304	37.61222	38.59675	58	44	323.31	1.355E+12	ACAN	Core matrisome	Proteoglycans
38.13351	37.11458	37.2389	40	40	323.31	8.169E+11	BGN	Core matrisome	Proteoglycans
34.66681	34.18016	34.82022	28	28	323.31	1.0685E+11	CHAD	Core matrisome	Proteoglycans
31.82092	31.91592	32.16261	22	22	241.79	17083000000	CHADL	Core matrisome	Proteoglycans
35.1541	34.74685	35.72059	35	35	323.31	1.1239E+11	DCN	Core matrisome	Proteoglycans
32.80178	32.10109	32.7333	15	15	148.23	14444000000	EPYC	Core matrisome	Proteoglycans
36.92316	36.52988	37.11206	18	17	323.31	4.5392E+11	FMOD	Core matrisome	Proteoglycans
37.48547	37.41266	37.4916	35	35	323.31	1.1332E+12	HAPLN1	Core matrisome	Proteoglycans
34.53427	34.64431	34.97383	16	16	119.67	1.4593E+11	HAPLN3	Core matrisome	Proteoglycans
34.04669	33.70275	34.25772	43	43	323.31	95011000000	HSPG2	Core matrisome	Proteoglycans
34.92937	34.986	33.65063	25	25	323.31	3.0026E+11	PRELP	Core matrisome	Proteoglycans
28.4305	30.16231	29.84559	10	10	74.382	1862600000	VCAN	Core matrisome	Proteoglycans
31.20362	31.68177	29.87093	12	12	78.173	5350600000	OGN	Core matrisome	Proteoglycans
26.40659	26.69445	NaN	10	10	76.111	3949200000	CD109	Matrisome-associated	ECM Regulators
27.79699	28.27604	28.57442	6	6	41.522	1867200000	HTRA1	Matrisome-associated	ECM Regulators
31.8928	32.0187	32.53362	25	24	238.19	18480000000	LOXL3	Matrisome-associated	ECM Regulators
26.99992	27.83382	NaN	10	10	77.139	1743600000	MMP2	Matrisome-associated	ECM Regulators
31.13057	31.08398	31.15074	20	14	253.75	25164000000	P4HA1	Matrisome-associated	ECM Regulators
29.29228	29.55459	29.19371	14	1	164.71	5652300000	P4HA2	Matrisome-associated	ECM Regulators
28.66942	28.83222	27.57521	19	19	190.8	7962100000	PLOD1	Matrisome-associated	ECM Regulators
31.71166	31.71129	31.91114	30	30	323.31	34482000000	Plod2	Matrisome-associated	ECM Regulators
29.90627	29.92366	29.95975	15	15	122.04	7705000000	SERPINB9	Matrisome-associated	ECM Regulators
29.25149	30.0189	28.7358	14	14	132.22	4556300000	SERPINF1	Matrisome-associated	ECM Regulators
34.33338	33.72862	33.96748	18	18	323.31	3.3455E+11	SERPINH1	Matrisome-associated	ECM Regulators
26.82723	NaN	27.24391	9	9	89.398	1780800000	TGM2	Matrisome-associated	ECM Regulators
29.84833	29.6803	28.98888	13	13	158.01	8819200000	LEPRE1	Matrisome-associated	ECM Regulators
27.34486	27.61316	26.79067	13	13	173.79	7681200000	ANXA1	Matrisome-associated	ECM-affiliated Proteins
27.04396	27.13046	NaN	9	9	70.727	1791400000	ANXA11	Matrisome-associated	ECM-affiliated Proteins
31.33485	31.30128	30.8165	29	29	323.31	35792000000	ANXA2	Matrisome-associated	ECM-affiliated Proteins
29.58135	30.21466	NaN	9	8	103.12	10727000000	ANXA4	Matrisome-associated	ECM-affiliated Proteins
31.59997	31.77643	30.97972	21	20	293.02	46716000000	ANXA5	Matrisome-associated	ECM-affiliated Proteins
29.78793	29.69486	NaN	31	31	242.73	12276000000	ANXA6	Matrisome-associated	ECM-affiliated Proteins
29.40718	29.40288	29.82561	4	4	76.867	1352900000	C1QA	Matrisome-associated	ECM-affiliated Proteins
30.31948	30.5904	30.73627	5	5	106.71	3252400000	C1QB	Matrisome-associated	ECM-affiliated Proteins
30.83914	31.02419	31.23438	6	6	60.613	4291200000	C1QC	Matrisome-associated	ECM-affiliated Proteins
32.87992	32.88131	33.0901	11	11	142.19	29212000000	CLEC3A	Matrisome-associated	ECM-affiliated Proteins
28.63457	NaN	28.47588	2	2	87.663	1712600000	CLEC3B	Matrisome-associated	ECM-affiliated Proteins
27.03601	27.01063	NaN	21	21	194.85	4834300000	CSPG4	Matrisome-associated	ECM-affiliated Proteins

29.52707	28.75344	28.47104	8	8	151.35	1179500000	GREM1	Matrisome-associated	ECM-affiliated Proteins
28.28313	28.25966	28.48999	3	3	19.077	2403500000	CCL16	Matrisome-associated	Secreted Factors
31.16327	31.38087	31.4608	7	7	66.002	5736300000	FRZB	Matrisome-associated	Secreted Factors
27.28542	NaN	26.12776	5	5	43.366	2943100000	IL17B	Matrisome-associated	Secreted Factors
26.12825	NaN	27.26901	2	2	11.503	209070000	SFRP5	Matrisome-associated	Secreted Factors
NaN	27.63083	27.01041	32	16	323.31	23890000000	ACL	#N/A	#N/A
29.71076	29.7427	28.31709	10	10	116	18428000000	ACP5	#N/A	#N/A
29.67649	29.35252	NaN	22	1	62.619	18211000000	ACTA1	#N/A	#N/A
33.54697	33.56309	33.69696	28	9	323.31	2.5729E+11	ACTB	#N/A	#N/A
29.37198	29.32034	27.27711	31	23	323.31	11522000000	ACTN1	#N/A	#N/A
26.35864	26.82238	25.92125	4	4	28.648	491890000	AKR1A1	#N/A	#N/A
30.36609	30.38154	30.04049	40	36	323.31	92479000000	ALB	#N/A	#N/A
28.59071	29.15323	NaN	5	4	41.231	2872100000	ALDOC	#N/A	#N/A
27.51209	27.65704	NaN	6	6	52.133	1546600000	ANG	#N/A	#N/A
26.59818	27.03926	NaN	3	3	44.396	1560300000	ARPC3	#N/A	#N/A
30.32549	30.53325	30.3004	23	23	208.38	30242000000	ATP5A1	#N/A	#N/A
29.73875	29.98915	29.03197	15	15	209.77	19781000000	ATP5B	#N/A	#N/A
28.16452	27.72592	28.36499	4	4	56.292	2271600000	CALM1	#N/A	#N/A
30.23843	30.67985	30.46918	12	12	98.089	11352000000	CALR	#N/A	#N/A
28.83358	28.50184	28.01792	9	9	115.77	6296800000	CALU	#N/A	#N/A
26.84589	26.9438	26.70833	10	10	86.254	3408300000	CANX	#N/A	#N/A
25.66611	25.84127	NaN	12	12	98.273	2274400000	CCT3	#N/A	#N/A
27.51232	27.39084	26.93179	10	10	64.906	2755600000	CCT6	#N/A	#N/A
28.73989	29.25487	29.61868	4	4	31.318	2672500000	CDH1	#N/A	#N/A
26.72598	27.33433	NaN	16	16	158.89	4268700000	CERCAM	#N/A	#N/A
27.05331	27.6487	27.3463	6	6	41.07	934250000	PHGDH	#N/A	#N/A
31.85073	31.96013	31.46349	18	18	195.3	7843600000	CHI3L1	#N/A	#N/A
29.9901	29.85039	28.20965	20	20	323.31	27773000000	MAN1A1	#N/A	#N/A
28.46115	28.88951	28.00747	27	27	197.12	7037500000	CLTC	#N/A	#N/A
28.50843	28.10159	28.0018	17	17	323.31	6512300000	CLU	#N/A	#N/A
28.67738	29.12903	NaN	24	24	174.45	5735700000	COPA	#N/A	#N/A
28.30352	28.5386	27.28419	19	19	166.35	4734800000	COPB2	#N/A	#N/A
26.89435	27.68525	NaN	5	5	40.511	2004400000	COPG1	#N/A	#N/A
28.57697	28.98014	28.20494	8	8	80.684	927050000	CPXM1	#N/A	#N/A
29.60256	29.57735	29.59174	8	8	61.47	1630700000	CYTL1	#N/A	#N/A
28.71908	28.85852	28.85881	7	7	49.739	4142300000	DDOST	#N/A	#N/A
27.41836	27.28577	NaN	11	9	88.717	2432700000	DDX17	#N/A	#N/A
30.53353	30.40507	30.0397	32	29	323.31	30683000000	DES	#N/A	#N/A
26.49023	27.87947	26.2029	19	19	154.79	4473500000	DHX9	#N/A	#N/A
27.5969	27.82341	28.1882	5	5	35.43	1499100000	DPYSL2	#N/A	#N/A
32.43204	31.86765	32.4023	19	19	179.55	75663000000	EEF1A	#N/A	#N/A
29.07104	29.25147	28.99375	11	11	84.006	7925800000	EEF1G	#N/A	#N/A
30.44085	31.03151	30.00531	32	31	285.65	23747000000	EEF2	#N/A	#N/A
27.83726	27.37882	27.97136	18	8	182.43	7777200000	EIF4A1	#N/A	#N/A
30.14746	29.97992	30.45248	17	15	312.31	12254000000	ENO1	#N/A	#N/A
28.74577	28.66811	28.96389	4	2	31.89	3502000000	ENO3	#N/A	#N/A
29.47297	29.83855	29.54698	11	10	99.671	16645000000	FKBP10	#N/A	#N/A

28.78469	NaN	28.6513	12	11	87.956	7753900000	FKBP9	#N/A	#N/A
27.68398	28.38989	NaN	4	4	23.905	1576500000	FLNC	#N/A	#N/A
26.91764	27.6401	NaN	7	7	49.994	1953200000	GALE	#N/A	#N/A
29.3138	28.01473	28.29697	23	23	204.23	6940300000	GANAB	#N/A	#N/A
32.67072	33.13063	32.48996	21	19	323.31	78498000000	GAPDH	#N/A	#N/A
26.61765	26.31986	NaN	25	14	205.17	8535100000	GBF1	#N/A	#N/A
26.69737	26.93191	26.72507	9	4	29.635	473930000	GDI1	#N/A	#N/A
28.07989	27.91131	28.97358	10	5	73.41	2562800000	GDI2	#N/A	#N/A
28.54422	29.02707	28.52683	23	1	200.56	8690000000	GFPT1	#N/A	#N/A
28.37065	29.30014	27.58527	13	13	129.3	8457300000	GNB2L1	#N/A	#N/A
27.82857	28.12785	26.84434	10	10	85.308	3169300000	GOT2	#N/A	#N/A
27.32328	27.36836	NaN	9	9	65.849	1277500000	GPI	#N/A	#N/A
30.94433	30.74695	31.33069	29	29	276.11	28153000000	GRP-58	#N/A	#N/A
30.58585	30.40669	30.47305	19	19	202.4	10286000000	GSN	#N/A	#N/A
27.47143	27.38435	NaN	6	6	45.982	1628700000	H1FX	#N/A	#N/A
31.60302	30.56747	32.04013	5	1	104.75	38764000000	H2AFX	#N/A	#N/A
32.83019	32.81027	33.73832	10	10	71.035	1.165E+11	H3F3A	#N/A	#N/A
31.13944	30.53621	31.68119	10	10	155.19	1.0671E+11	HBA	#N/A	#N/A
32.50429	31.7906	32.36497	16	8	323.31	3.1071E+11	HBB	#N/A	#N/A
26.91787	27.15943	27.55618	15	15	115.23	2626600000	HDLBP	#N/A	#N/A
27.40592	27.82633	NaN	9	9	64.93	557920000	HHIPL2	#N/A	#N/A
31.11607	31.10368	32.18255	17	10	92.793	32376000000	HIST1H1B	#N/A	#N/A
33.8561	33.75304	34.88699	20	7	182.26	1.1772E+11	HIST1H1T	#N/A	#N/A
33.91874	33.63168	34.03878	13	3	214.7	2.1713E+11	HIST1H2BA	#N/A	#N/A
34.072	33.42492	33.33338	15	15	167.79	2.4993E+11	HIST1H4A	#N/A	#N/A
29.27886	28.98905	29.92719	13	3	21.645	9990000000	HIST3H2BB	#N/A	#N/A
NaN	27.68325	28.16686	8	4	68.695	2245500000	HNRNPA2B1	#N/A	#N/A
27.60357	27.61947	28.36328	15	15	118.35	4537100000	HNRNPM	#N/A	#N/A
29.31592	29.86586	28.73215	17	17	147.87	8575600000	HNRNPU	#N/A	#N/A
31.07527	31.13357	30.39693	26	17	323.31	30435000000	HSP90AA1	#N/A	#N/A
31.80132	31.80309	31.48779	33	31	323.31	48917000000	HSP90B1	#N/A	#N/A
27.8496	28.33743	26.87173	16	7	115.7	1844000000	HSPA1A	#N/A	#N/A
31.49496	31.29038	31.27042	34	32	323.31	46947000000	HSPA5	#N/A	#N/A
26.78019	28.10225	27.01924	16	16	162.89	10002000000	HSPD1	#N/A	#N/A
27.38311	26.89412	26.59106	9	0	68.35	9845100000	IGHG	#N/A	#N/A
32.98924	32.68288	33.09046	31	31	323.31	20828000000	IL1RAP	#N/A	#N/A
26.81787	27.09476	NaN	13	13	93.836	1090300000	IQGAP1	#N/A	#N/A
28.30691	28.57542	29.12317	8	8	69.481	934570000	K1C9	#N/A	#N/A
29.36317	29.36576	29.68913	12	6	120.81	2112900000	K2C1	#N/A	#N/A
28.07163	27.66085	28.81381	9	8	70.186	991110000	KRT10	#N/A	#N/A
30.6748	30.87884	30.80855	15	13	126.1	17606000000	LDHA	#N/A	#N/A
28.23375	28.52739	28.15649	8	3	44.76	2986600000	LDHB	#N/A	#N/A
32.24181	32.24329	32.19287	5	5	50.349	24717000000	LECT2	#N/A	#N/A
30.74951	30.75031	31.08474	30	1	288.53	13692000000	LMNA	#N/A	#N/A
30.26002	30.13675	29.69765	15	6	45.068	26403000000	LOC100154783	#N/A	#N/A
31.53691	31.72716	31.60731	27	27	323.31	86014000000	LOC100156689	#N/A	#N/A
37.36177	36.87062	35.88445	4	4	207.32	7.9947E+11	LOC100302368	#N/A	#N/A

30.66051	31.05381	31.23426	9	9	74.431	9184200000	LOC100510904	#N/A	#N/A
27.24254	27.86938	NaN	23	1	252.87	7078000000	LOC100516776	#N/A	#N/A
28.57924	NaN	29.605	7	7	68.388	11384000000	LOC100517228	#N/A	#N/A
27.34942	28.3598	NaN	11	11	93.326	3713100000	LOC100519984	#N/A	#N/A
30.32012	30.41901	29.65412	5	5	33.773	9254800000	LOC100523846	#N/A	#N/A
31.43847	31.32442	31.9951	12	12	126.82	18367000000	LOC100626701	#N/A	#N/A
31.86784	32.09544	30.96534	10	10	69.362	8739200000	LOC100737120	#N/A	#N/A
31.72501	31.41705	31.47354	15	6	264.78	57354000000	LOC100737887	#N/A	#N/A
26.93764	26.77744	27.07153	2	2	15.113	853750000	LOC100738863	#N/A	#N/A
28.69694	29.25813	27.99026	6	6	70.58	5517200000	LOC102164134	#N/A	#N/A
NaN	30.33127	29.84313	3	3	19.787	2841000000	LOC102165291	#N/A	#N/A
32.04238	31.46884	32.53095	14	14	220.35	22820000000	LOC102165939	#N/A	#N/A
30.09258	30.17176	31.22711	18	5	43.179	9224400000	LOC595122	#N/A	#N/A
28.40941	27.88943	27.11327	27	27	193.17	3279400000	LRP1	#N/A	#N/A
34.89938	34.48388	33.87298	16	4	323.31	64996000000	LYSC3	#N/A	#N/A
27.63277	28.18333	27.78463	9	9	70.856	1455300000	MFI2	#N/A	#N/A
28.46443	27.30382	27.73286	20	11	141.37	8078400000	MSN	#N/A	#N/A
28.40186	27.48577	NaN	5	5	70.046	5327000000	MYL6	#N/A	#N/A
25.35151	26.07063	NaN	4	4	27.518	475620000	MYO1C	#N/A	#N/A
28.84906	28.6102	29.256	8	4	61.131	8499500000	NME2	#N/A	#N/A
27.99156	27.45419	NaN	6	6	39.847	2721500000	NPM1	#N/A	#N/A
28.11709	28.42682	27.23517	16	16	152.03	5872600000	OAT	#N/A	#N/A
26.30172	26.10242	NaN	14	9	142.81	3284900000	PABPC1	#N/A	#N/A
25.93411	26.49881	NaN	8	7	50.692	1043500000	PAPSS1	#N/A	#N/A
30.17355	30.38463	30.57443	25	24	214.19	27433000000	PAPSS2	#N/A	#N/A
29.75774	30.18483	29.09821	31	31	282.8	19455000000	PDIA4	#N/A	#N/A
29.57933	29.32135	30.19202	13	13	184.03	8820900000	PDI-P5	#N/A	#N/A
27.50983	27.4929	26.74689	11	8	76.408	1665000000	PFKL	#N/A	#N/A
28.58068	28.71614	28.40617	13	11	107.3	1649000000	PFKP	#N/A	#N/A
29.11376	29.27673	29.99712	12	12	138.61	7244700000	PGAM1	#N/A	#N/A
30.62767	30.84229	30.54757	22	0	237.22	12687000000	PGK1	#N/A	#N/A
31.5993	31.87595	32.47528	18	18	188.41	29736000000	PKLR	#N/A	#N/A
29.59523	29.21799	30.16159	9	8	89.431	16435000000	PPIA	#N/A	#N/A
28.21127	28.58172	NaN	8	5	49.279	6868200000	PRDX1	#N/A	#N/A
28.13193	28.13001	27.70154	6	6	42.555	2883900000	PRDX2	#N/A	#N/A
29.97254	29.94712	28.60752	10	7	86.057	10038000000	PRDX4	#N/A	#N/A
29.20562	30.11917	28.40402	6	6	40.881	1882500000	PRDX6	#N/A	#N/A
27.81427	26.92343	26.87361	11	11	130.81	3223100000	PRKCSH	#N/A	#N/A
25.67047	25.99624	NaN	4	4	27.646	629210000	PRPS2	#N/A	#N/A
26.81336	NaN	27.11297	3	3	18.715	201080000	PXYLP1	#N/A	#N/A
27.97049	27.31562	27.39067	10	10	74.396	4235300000	RAN	#N/A	#N/A
30.10974	29.69056	29.33208	5	5	45.408	2722700000	RARRES2	#N/A	#N/A
28.50971	28.80698	28.69126	8	8	142.03	8716200000	RCN3	#N/A	#N/A
31.52	30.94196	31.43151	8	8	163.62	10890000000	RNASE4	#N/A	#N/A
29.30917	29.5583	29.59674	11	11	145.69	11088000000	RPL10	#N/A	#N/A
28.3198	NaN	28.78821	7	2	64.965	5413100000	RPL10A	#N/A	#N/A
28.14482	28.43595	29.51788	10	10	108.75	5713200000	RPL11	#N/A	#N/A

29.25163	29.1121	29.71741	8	8	80.759	10270000000	RPL13	#N/A	#N/A
28.71276	29.76387	29.25627	13	13	80.826	8108200000	RPL13A	#N/A	#N/A
29.26915	29.08134	29.2488	9	9	63.036	10171000000	RPL14	#N/A	#N/A
28.44608	29.23569	NaN	8	8	70.409	9378000000	RPL15	#N/A	#N/A
29.43432	29.57744	30.15025	7	7	108.74	15583000000	RPL18	#N/A	#N/A
29.35708	29.03178	NaN	11	11	78.765	10878000000	RPL18A	#N/A	#N/A
26.77718	27.11068	28.16466	5	5	68.931	5758500000	RPL19	#N/A	#N/A
29.51122	29.42946	29.44608	7	6	63.332	8971600000	RPL22	#N/A	#N/A
27.2261	27.07551	NaN	3	3	21.804	2315600000	RPL23	#N/A	#N/A
27.6083	27.71745	NaN	9	9	64.07	7681600000	RPL23A	#N/A	#N/A
27.04635	27.67889	NaN	5	5	36.69	6580800000	RPL24	#N/A	#N/A
27.80329	28.14807	27.92914	8	8	63.301	6320600000	RPL27	#N/A	#N/A
29.61523	29.90067	30.75772	17	17	135.71	12049000000	RPL3	#N/A	#N/A
27.94218	28.26857	28.02512	7	7	60.51	3751600000	RPL30	#N/A	#N/A
29.2184	29.14287	30.14029	9	9	55.756	9409000000	RPL35A	#N/A	#N/A
29.13563	28.23023	30.06021	22	10	186.3	17135000000	RPL4	#N/A	#N/A
28.96097	28.89209	28.90486	10	10	88.252	8693100000	RPL5	#N/A	#N/A
30.43619	30.49629	30.76809	18	18	225.46	40983000000	RPL6	#N/A	#N/A
29.05636	29.64065	27.98506	14	7	108.18	13182000000	RPL7	#N/A	#N/A
29.06992	29.26944	29.17358	6	6	48.737	11490000000	RPL7A	#N/A	#N/A
29.27888	29.63093	29.96884	13	13	98.211	19941000000	RPL8	#N/A	#N/A
28.50764	29.05204	27.04562	6	6	44.379	6601000000	RPL9	#N/A	#N/A
28.44482	28.31207	NaN	8	8	79.191	5270300000	RPLP0	#N/A	#N/A
29.10167	29.41663	28.94053	17	17	134.04	7482500000	RPN1	#N/A	#N/A
29.14029	29.82789	29.52172	14	14	99.938	11454000000	RPS11	#N/A	#N/A
28.23713	28.15393	NaN	6	6	45.377	3466200000	RPS13	#N/A	#N/A
30.0575	30.42832	30.0817	12	12	91.65	14745000000	RPS16	#N/A	#N/A
28.25997	27.65185	NaN	3	3	21.802	5780300000	RPS17	#N/A	#N/A
29.1116	29.54988	NaN	13	13	107.33	11447000000	RPS18	#N/A	#N/A
27.49899	27.41119	28.58978	10	10	90.457	3364900000	RPS19	#N/A	#N/A
29.70197	29.90441	29.80226	12	12	83.13	12547000000	RPS2	#N/A	#N/A
28.51171	28.27799	28.53382	4	4	32.479	4437700000	RPS20	#N/A	#N/A
27.63027	28.1155	NaN	6	6	53.499	11253000000	RPS25	#N/A	#N/A
29.8752	30.33756	28.88792	21	21	172.52	15605000000	RPS3	#N/A	#N/A
30.08512	30.45973	29.99577	18	18	141.28	17611000000	RPS3A	#N/A	#N/A
30.05414	30.09472	30.5538	16	16	157.93	21434000000	Rps4	#N/A	#N/A
28.34621	NaN	28.7024	8	8	86.23	5280900000	RPS5	#N/A	#N/A
28.6804	29.65395	29.0352	15	7	124.15	13145000000	RPS6	#N/A	#N/A
29.34993	29.59295	30.33639	13	13	179.15	11049000000	RPS8	#N/A	#N/A
28.84781	29.30493	27.86744	13	2	85.755	9704400000	RPS9	#N/A	#N/A
28.28065	28.95543	27.68592	11	11	149.77	4991100000	RPSA	#N/A	#N/A
28.74727	28.93787	28.30008	26	26	234.95	9770500000	RRBP1	#N/A	#N/A
28.93019	29.29691	28.81351	13	13	123.39	4748600000	SCIN	#N/A	#N/A
26.26275	26.43111	NaN	5	5	32.853	819690000	SEPT9	#N/A	#N/A
28.3887	28.806	NaN	9	3	60.283	11981000000	SLC25A6	#N/A	#N/A
27.43651	27.33705	28.00667	4	4	25.233	478390000	SRSF1	#N/A	#N/A
27.44237	27.56376	NaN	2	2	11.84	1173800000	SRSF2	#N/A	#N/A

26.9438	27.17217	NaN	2	2	19.876	439790000	SRSF7	#N/A	#N/A
26.94827	27.09456	26.40056	4	4	34.982	3151900000	SSR4	#N/A	#N/A
28.52099	28.37844	29.11317	13	13	98.54	3383500000	TKT	#N/A	#N/A
28.28445	27.4753	28.88256	5	5	39.731	3811200000	TMED10	#N/A	#N/A
28.51009	28.72722	27.99405	9	9	116.04	3631600000	TPI1	#N/A	#N/A
30.73925	30.36328	30.11706	15	0	301.26	28470000000	TUBA1B	#N/A	#N/A
30.72029	30.94942	29.79707	17	2	263.11	33599000000	TUBB	#N/A	#N/A
26.53677	27.09325	26.29365	17	3	36.604	911570000	TUBB1	#N/A	#N/A
29.81317	30.25462	29.45617	20	20	268.3	17166000000	UGDH	#N/A	#N/A
29.10059	29.54955	28.62226	16	16	121.36	2597000000	UGP2	#N/A	#N/A
27.42502	28.21739	NaN	7	7	73.542	4733800000	VDAC2	#N/A	#N/A
26.5077	26.71424	NaN	7	2	42.662	1175400000	YWHAB	#N/A	#N/A
28.10335	28.32006	27.25241	7	5	128.12	1643100000	YWHAZ	#N/A	#N/A
32.97946	32.8334	33.35928	35	35	323.31	1.1865E+11	Uncharacterized	#N/A	#N/A
30.18423	29.72607	30.37067	24	15	247.17	26045000000	Uncharacterized	#N/A	#N/A
31.13479	31.48015	30.9262	12	12	162.18	40411000000	Uncharacterized	#N/A	#N/A
31.36448	31.39703	31.92142	14	14	159.62	40425000000	Uncharacterized	#N/A	#N/A
30.40832	30.05659	30.58388	4	4	38.913	33554000000	Uncharacterized	#N/A	#N/A

Table S3. List of proteins detected in Growth Plate ECM using Mass Spectrometry

LFQ intensity GP_1	LFQ intensity GP_2	LFQ intensity GP_3	Peptides	Unique peptides	Score	Intensity	Gene name	Division Matrisome	Subcategory Matrisome
31.86964	31.8814	31.6793	6	6	68.709	22808000000	COL10A1	Core matrisome	Collagens
31.4565	31.47798	31.69839	15	14	191.17	20304000000	COL11A1	Core matrisome	Collagens
34.72243	34.7448	34.49816	39	38	323.31	2.3936E+11	COL11A2	Core matrisome	Collagens
29.84313	29.83189	30.15388	8	3	80.797	9189500000	COL15A1	Core matrisome	Collagens
30.76596	29.71094	29.06856	4	4	31.884	10193000000	COL1A1	Core matrisome	Collagens
31.61048	31.57172	31.32726	13	13	93.924	20345000000	COL1A2	Core matrisome	Collagens
27.16394	26.91354	NaN	3	3	19.264	995870000	COL27A1	Core matrisome	Collagens
34.98261	35.09969	34.65598	17	16	323.31	2.6774E+11	COL2A1	Core matrisome	Collagens
29.22621	28.74942	28.34782	5	5	39.442	3531900000	COL2A1	Core matrisome	Collagens
28.57932	28.54753	28.47022	3	3	20.092	2514200000	COL3A1	Core matrisome	Collagens
31.0922	30.27653	30.12509	12	12	101.03	17787000000	COL6A1	Core matrisome	Collagens
27.7267	27.69929	NaN	6	6	82.783	2976300000	COL6A1	Core matrisome	Collagens
30.08347	29.82488	29.70956	3	3	39.012	12479000000	COL6A1	Core matrisome	Collagens
31.61127	31.85133	31.6842	29	29	297.87	51108000000	COL6A2	Core matrisome	Collagens
33.5103	33.46405	33.56751	122	122	323.31	1.7419E+11	COL6A3	Core matrisome	Collagens
34.08686	34.02952	34.07758	21	21	323.31	1.5189E+11	COL9A1	Core matrisome	Collagens
32.46449	32.7317	32.76129	5	5	82.195	48229000000	COL9A2	Core matrisome	Collagens
28.68949	28.83506	29.62207	9	9	59.91	6513200000	COL16A1	Core matrisome	Collagens
NaN	25.30215	26.3369	5	5	37.135	266920000	AGRN	Core matrisome	ECM Glycoproteins
27.55764	NaN	27.56986	30	2	96.405	2312400000	COMP	Core matrisome	ECM Glycoproteins
35.4087	35.37205	35.21056	41	13	323.31	5.5647E+11	COMP	Core matrisome	ECM Glycoproteins
NaN	27.38755	27.3407	3	3	24.892	658540000	CTGF	Core matrisome	ECM Glycoproteins
30.50076	30.46509	30.83289	6	6	67.35	19448000000	CTHRC1	Core matrisome	ECM Glycoproteins
32.43584	32.43445	32.44285	15	15	153.38	45634000000	EDIL3	Core matrisome	ECM Glycoproteins
27.72605	27.68472	27.82675	3	3	30.724	1966700000	EFEMP2	Core matrisome	ECM Glycoproteins
28.07173	27.05992	NaN	12	12	96.492	1429300000	EMILIN1	Core matrisome	ECM Glycoproteins
29.90999	29.84417	30.00838	17	17	136.14	21175000000	FBLN7	Core matrisome	ECM Glycoproteins
30.35867	30.32539	30.14151	11	6	43.315	7939300000	FGA	Core matrisome	ECM Glycoproteins
33.81373	33.74495	33.73217	33	33	323.31	89384000000	FGB	Core matrisome	ECM Glycoproteins
27.18641	26.78856	26.74484	1	1	20.756	769450000	FGB	Core matrisome	ECM Glycoproteins
35.42264	35.40768	35.37347	88	88	323.31	3.4305E+11	FN1	Core matrisome	ECM Glycoproteins
29.08096	29.25836	29.02675	6	6	46.117	3586700000	IBSP	Core matrisome	ECM Glycoproteins
27.11486	26.84194	26.74881	7	7	47.443	765570000	LAMA4	Core matrisome	ECM Glycoproteins
27.36169	26.73725	26.77994	9	9	61.165	977500000	LAMB2	Core matrisome	ECM Glycoproteins
32.70837	32.74819	32.39922	39	39	323.31	2.962E+11	MATN1	Core matrisome	ECM Glycoproteins
29.93115	30.22986	30.30954	12	12	117.15	10296000000	MATN2	Core matrisome	ECM Glycoproteins
35.80222	35.58212	35.25053	33	33	323.31	5.7601E+11	MATN3	Core matrisome	ECM Glycoproteins
29.42584	29.22568	29.84169	28	28	259.09	36329000000	MATN4	Core matrisome	ECM Glycoproteins
32.78384	32.7243	32.82618	24	24	274.88	60988000000	MFGE8	Core matrisome	ECM Glycoproteins
26.28673	NaN	26.15275	8	8	79.437	1390000000	PCOLCE	Core matrisome	ECM Glycoproteins
26.68097	26.99981	26.5225	8	8	61.368	1149700000	PCOLCE2	Core matrisome	ECM Glycoproteins
31.19712	31.32646	31.02518	9	9	79.112	17480000000	SPARC	Core matrisome	ECM Glycoproteins
28.41183	28.2502	28.56456	11	11	82.189	3741200000	SRPX	Core matrisome	ECM Glycoproteins
25.87488	26.38364	25.86964	23	23	197.48	9971900000	SRPX2	Core matrisome	ECM Glycoproteins

27.76421	28.29754	28.00421	28	28	289.22	33968000000	TGFBI	Core matrisome	ECM Glycoproteins
34.71365	34.62402	34.63011	62	61	323.31	3.0238E+11	THBS1	Core matrisome	ECM Glycoproteins
31.43072	31.24768	31.42397	18	16	130.19	22253000000	THBS3	Core matrisome	ECM Glycoproteins
31.51789	31.43624	31.54954	64	18	323.31	80969000000	TNC	Core matrisome	ECM Glycoproteins
30.44312	30.49123	30.63504	22	22	323.31	20351000000	VIT	Core matrisome	ECM Glycoproteins
29.80852	29.73379	29.88495	11	11	103.91	5737200000	VTN	Core matrisome	ECM Glycoproteins
33.49334	33.61204	33.53612	21	21	306.7	75371000000	FGG	Core matrisome	ECM Glycoproteins
36.81024	36.73618	36.44648	58	44	323.31	1.355E+12	ACAN	Core matrisome	Proteoglycans
36.52052	36.35834	35.9529	40	40	323.31	8.169E+11	BGN	Core matrisome	Proteoglycans
33.35192	33.34863	33.10676	28	28	323.31	1.0685E+11	CHAD	Core matrisome	Proteoglycans
30.44983	30.62706	30.70561	22	22	241.79	17083000000	CHADL	Core matrisome	Proteoglycans
32.34226	32.33103	32.03184	35	35	323.31	1.1239E+11	DCN	Core matrisome	Proteoglycans
28.46205	28.33735	28.20914	15	15	148.23	14444000000	EPYC	Core matrisome	Proteoglycans
34.86092	34.84973	34.79188	18	17	323.31	4.5392E+11	FMOD	Core matrisome	Proteoglycans
37.12328	37.12232	36.78877	35	35	323.31	1.1332E+12	HAPLN1	Core matrisome	Proteoglycans
33.24545	33.3598	33.21752	43	43	323.31	95011000000	HSPG2	Core matrisome	Proteoglycans
27.44624	27.18168	NaN	6	6	43.417	940010000	LUM	Core matrisome	Proteoglycans
35.23292	35.32456	35.24693	25	25	323.31	3.0026E+11	PRELP	Core matrisome	Proteoglycans
27.05051	NaN	27.03297	12	12	78.173	5350600000	OGN	Core matrisome	Proteoglycans
28.08618	28.27177	28.14424	3	3	25.29	1755100000	PRG3	Core matrisome	Proteoglycans
29.30704	29.25476	29.31685	19	1	141.52	4029300000	A2M	Matrisome-associated	ECM Regulators
29.43724	28.78687	29.14972	10	10	76.111	3949200000	CD109	Matrisome-associated	ECM Regulators
27.32406	27.14433	27.43928	4	4	25.405	1035400000	CTSD	Matrisome-associated	ECM Regulators
27.53475	27.34036	27.64334	4	4	28.92	1157500000	CTSG	Matrisome-associated	ECM Regulators
27.66445	27.49823	27.6452	5	5	30.51	1205000000	CTSK	Matrisome-associated	ECM Regulators
28.23361	27.8337	28.13717	5	5	45.202	1763100000	ELANE	Matrisome-associated	ECM Regulators
28.31993	28.51717	28.41639	6	6	64.969	2173500000	F10	Matrisome-associated	ECM Regulators
31.34647	31.15225	31.39872	20	20	137.27	15980000000	F13A1	Matrisome-associated	ECM Regulators
26.61428	26.80993	26.9608	6	6	94.43	649080000	F2	Matrisome-associated	ECM Regulators
26.96521	26.8947	26.86242	5	5	30.383	781010000	HRG	Matrisome-associated	ECM Regulators
27.61723	27.38813	27.41321	6	6	41.522	1867200000	HTRA1	Matrisome-associated	ECM Regulators
26.01822	26.22992	26.23325	5	5	30.835	455390000	HTRA3	Matrisome-associated	ECM Regulators
26.8114	26.79984	27.13878	6	6	40.787	776720000	ITIH1	Matrisome-associated	ECM Regulators
26.4123	26.38237	26.7397	5	5	34.333	574570000	ITIH2	Matrisome-associated	ECM Regulators
27.34765	27.15316	27.24209	8	2	71.405	955180000	ITIH4	Matrisome-associated	ECM Regulators
26.84637	26.86773	26.73337	8	2	14.209	707960000	ITIH4	Matrisome-associated	ECM Regulators
30.5001	30.47711	30.66958	25	24	238.19	18480000000	LOXL3	Matrisome-associated	ECM Regulators
27.53519	27.8259	27.64231	7	6	103.44	1350600000	LOXL4	Matrisome-associated	ECM Regulators
27.8444	27.88116	28.03118	11	11	91.608	1540800000	MMP13	Matrisome-associated	ECM Regulators
27.51676	27.83141	28.05894	10	10	77.139	1743600000	MMP2	Matrisome-associated	ECM Regulators
27.62687	27.61512	27.87085	7	7	43.028	1295800000	MMP9	Matrisome-associated	ECM Regulators
31.67741	31.6751	31.51911	20	14	253.75	25164000000	P4HA1	Matrisome-associated	ECM Regulators
29.12832	29.29872	29.50457	14	1	164.71	5652300000	P4HA2	Matrisome-associated	ECM Regulators
27.75678	27.36695	27.61253	7	7	46.817	1335600000	PAMR1	Matrisome-associated	ECM Regulators
30.02406	29.79129	30.10986	19	19	190.8	7962100000	PLOD1	Matrisome-associated	ECM Regulators
31.96041	31.95989	31.88143	30	30	323.31	34482000000	Plod2	Matrisome-associated	ECM Regulators
30.06805	29.86781	30.08119	13	13	96.305	6500600000	PLOD3	Matrisome-associated	ECM Regulators

27.34934	27.44624	27.48116	7	7	48.654	1086400000	SERPINC1	Matrisome-associated	ECM Regulators
29.02327	29.17724	29.05391	14	14	132.22	4556300000	SERPINF1	Matrisome-associated	ECM Regulators
35.60673	35.64528	35.25188	18	18	323.31	3.3455E+11	SERPINH1	Matrisome-associated	ECM Regulators
27.5534	27.79947	28.05719	9	9	89.398	1780800000	TGM2	Matrisome-associated	ECM Regulators
30.17081	30.22699	30.06394	13	13	158.01	8819200000	LEPRE1	Matrisome-associated	ECM Regulators
26.7252	NaN	26.37607	3	3	19.936	495150000	LEPREL2	Matrisome-associated	ECM Regulators
29.68924	29.62697	29.56518	15	15	122.04	7705000000	SERPINB9	Matrisome-associated	ECM Regulators
30.26338	29.81638	30.25169	13	13	173.79	7681200000	ANXA1	Matrisome-associated	ECM-affiliated Proteins
27.87467	27.85317	27.91359	9	9	70.727	1791400000	ANXA11	Matrisome-associated	ECM-affiliated Proteins
32.21393	32.22866	32.23914	29	29	323.31	35792000000	ANXA2	Matrisome-associated	ECM-affiliated Proteins
30.03957	30.40507	30.29702	9	8	103.12	10727000000	ANXA4	Matrisome-associated	ECM-affiliated Proteins
32.66708	32.66643	32.40561	21	20	293.02	46716000000	ANXA5	Matrisome-associated	ECM-affiliated Proteins
30.7024	30.50398	30.48164	31	31	242.73	12276000000	ANXA6	Matrisome-associated	ECM-affiliated Proteins
31.3205	30.4074	30.02115	16	16	129.91	10928000000	ANXA8	Matrisome-associated	ECM-affiliated Proteins
28.34024	28.1053	28.5023	6	6	48.191	2113500000	C1QTNF3	Matrisome-associated	ECM-affiliated Proteins
29.93649	30.0177	30.14601	9	9	112	6667900000	CLEC11A	Matrisome-associated	ECM-affiliated Proteins
30.97965	31.01319	31.14224	11	11	142.19	29212000000	CLEC3A	Matrisome-associated	ECM-affiliated Proteins
27.43118	27.30583	27.42806	2	2	87.663	1712600000	CLEC3B	Matrisome-associated	ECM-affiliated Proteins
29.56518	29.41272	29.47785	21	21	194.85	4834300000	CSPG4	Matrisome-associated	ECM-affiliated Proteins
25.20717	25.26567	NaN	2	2	11.626	207290000	HPX	Matrisome-associated	ECM-affiliated Proteins
27.25629	27.44443	NaN	2	2	14.171	802540000	LGALS1	Matrisome-associated	ECM-affiliated Proteins
27.41941	27.73389	27.81464	4	4	26.907	1295200000	LMAN1	Matrisome-associated	ECM-affiliated Proteins
29.91997	29.79854	29.8561	17	16	285.18	5931200000	ANGPTL2	Matrisome-associated	Secreted Factors
28.34807	28.48416	28.43865	7	7	48.848	2235900000	ANGPTL5	Matrisome-associated	Secreted Factors
28.20969	28.06322	28.11615	3	3	19.077	2403500000	CCL16	Matrisome-associated	Secreted Factors
28.50832	28.83723	28.79272	5	5	43.366	2943100000	IL17B	Matrisome-associated	Secreted Factors
27.60717	27.43333	27.28374	2	2	15.483	1119300000	S100A12	Matrisome-associated	Secreted Factors
28.85332	28.34236	27.83117	4	4	28.869	2188500000	S100A8	Matrisome-associated	Secreted Factors
27.90438	27.82917	27.3864	4	4	29.775	1405700000	S100A9	Matrisome-associated	Secreted Factors
29.14664	28.26222	28.29255	3	3	38.991	2825200000	S100A10	Matrisome-associated	Secreted Factors
31.50323	31.3741	32.4775	32	16	323.31	23890000000	ACL	#N/A	#N/A
28.40718	28.47073	28.71954	10	10	120.58	2439900000	ACO2	#N/A	#N/A
24.50567	24.38476	24.31299	2	2	12.458	132160000	ACOT9	#N/A	#N/A
31.17003	31.28234	31.66941	10	10	116	18428000000	ACP5	#N/A	#N/A
31.2302	31.40806	31.27075	22	1	62.619	18211000000	ACTA1	#N/A	#N/A
34.96073	35.22834	35.03014	28	9	323.31	2.5729E+11	ACTB	#N/A	#N/A
30.62235	30.56837	30.66391	31	23	323.31	11522000000	ACTN1	#N/A	#N/A
27.39591	27.38862	27.31207	4	4	36.755	1020900000	ACTR2	#N/A	#N/A
28.14676	28.19075	28.45525	6	6	44.15	2250900000	ACTR3	#N/A	#N/A
25.76152	26.10079	NaN	4	4	23.815	326700000	AHNAK	#N/A	#N/A
32.43261	32.47528	32.3395	11	11	133.55	34306000000	AHSG	#N/A	#N/A
26.14235	NaN	26.11265	3	3	19.016	399960000	AK1	#N/A	#N/A
25.85201	25.71552	25.88143	4	4	28.648	491890000	AKR1A1	#N/A	#N/A
26.09394	NaN	26.67425	4	4	28.795	431010000	AKT1	#N/A	#N/A
30.407	30.28571	30.18092	6	2	13.301	7975300000	ALB	#N/A	#N/A
33.91421	33.70718	33.67167	40	36	323.31	92479000000	ALB	#N/A	#N/A
27.29973	27.08091	27.53208	8	8	59.935	1137800000	ALDH18A1	#N/A	#N/A

27.97224	28.1247	28.3333	8	8	54.406	1939800000	ALDH1A1	#N/A	#N/A
27.74817	28.05424	28.11664	5	4	41.231	2872100000	ALDOC	#N/A	#N/A
29.22741	29.27881	29.81293	4	2	31.685	4330600000	ALPL	#N/A	#N/A
27.51345	27.549	27.78594	6	6	52.133	1546600000	ANG	#N/A	#N/A
25.66568	NaN	25.75277	2	2	14.09	314070000	AP1B1	#N/A	#N/A
28.76572	28.83397	28.86142	9	9	65.026	2843300000	APOA1	#N/A	#N/A
28.38496	28.48999	28.67539	5	5	43.398	2724500000	APOD	#N/A	#N/A
27.89053	27.86396	28.13305	7	7	46.807	1532200000	APOE	#N/A	#N/A
27.59939	27.91199	27.65226	6	6	54.459	1312500000	APOH	#N/A	#N/A
28.12544	28.03852	28.27586	9	9	81.385	2176200000	ARCN1	#N/A	#N/A
29.03514	29.21313	29.30767	3	2	28.757	3675200000	ARF4	#N/A	#N/A
NaN	25.48533	25.7572	6	6	52.163	346350000	ARHGDIA	#N/A	#N/A
28.05284	27.63464	27.92093	7	7	54.992	1463400000	ARPC1B	#N/A	#N/A
27.67553	27.9921	27.48078	3	3	44.396	1560300000	ARPC3	#N/A	#N/A
27.32096	26.96576	26.70741	3	3	24.318	809150000	ARPC4	#N/A	#N/A
26.25915	NaN	26.72546	7	7	53.157	459640000	ATP12A	#N/A	#N/A
31.97354	32.04908	31.99112	23	23	208.38	30242000000	ATP5A1	#N/A	#N/A
31.24949	31.35574	31.66936	15	15	209.77	19781000000	ATP5B	#N/A	#N/A
27.27985	28.9911	28.83204	3	3	21.885	2039300000	ATP5H	#N/A	#N/A
25.96825	25.91798	NaN	2	2	14.475	355080000	ATP5J2	#N/A	#N/A
28.86573	28.9223	28.95407	5	5	49.189	3055600000	ATP5O	#N/A	#N/A
27.64293	27.84631	28.24095	8	8	112.34	1492800000	ATP6V1A	#N/A	#N/A
26.00288	25.93944	NaN	5	5	32.906	363630000	ATP6V1B1	#N/A	#N/A
28.55248	28.50714	28.84903	6	6	60.611	2449800000	AZU1	#N/A	#N/A
26.69869	26.603	26.71135	5	5	33.538	675660000	BAT1	#N/A	#N/A
26.73828	26.84733	26.86124	6	6	42.834	735130000	BF	#N/A	#N/A
28.42878	28.50211	28.43269	3	3	20.136	2337200000	BSG	#N/A	#N/A
25.16909	25.09225	25.44881	3	3	18.108	241470000	BUB3	#N/A	#N/A
25.5576	NaN	25.60659	3	3	18.631	251890000	BZW1	#N/A	#N/A
26.94257	26.84326	27.0403	2	2	21.04	773410000	C19ORF10	#N/A	#N/A
24.60371	24.83205	NaN	2	2	13.026	182530000	C2ORF40	#N/A	#N/A
28.88963	28.97378	29.09966	19	5	120.82	3205600000	C3	#N/A	#N/A
NaN	24.20142	23.55274	2	2	12.895	64246000	C4	#N/A	#N/A
26.16638	NaN	26.51904	3	3	19.639	481590000	C4BPA	#N/A	#N/A
27.19141	NaN	27.07439	6	6	44.987	760990000	C9	#N/A	#N/A
25.49201	25.43705	26.25838	3	3	20.858	331510000	CA2	#N/A	#N/A
28.25354	27.89678	27.7916	4	4	56.292	2271600000	CALM1	#N/A	#N/A
30.42882	30.17021	30.26081	12	12	98.089	11352000000	CALR	#N/A	#N/A
29.77508	29.60851	29.64979	9	9	115.77	6296800000	CALU	#N/A	#N/A
28.87367	29.01654	28.70091	10	10	86.254	3408300000	CANX	#N/A	#N/A
26.76471	26.8853	NaN	3	3	24.638	599280000	CAPZA	#N/A	#N/A
26.53769	26.73867	26.79724	6	6	42.979	656780000	CAT	#N/A	#N/A
27.71529	27.86189	27.81207	5	5	42.405	1382500000	CBF-A	#N/A	#N/A
29.01361	29.70393	29.73656	17	17	133.16	4991400000	CCDC80	#N/A	#N/A
28.57672	28.15943	28.44825	12	12	98.273	2274400000	CCT3	#N/A	#N/A
28.28542	27.92892	28.23713	8	8	51.005	2101400000	CCT4	#N/A	#N/A
27.56776	27.13516	27.42246	9	9	60.341	1203000000	CCT5	#N/A	#N/A

28.54252	28.14122	28.53263	10	10	64.906	2755600000	CCT6	#N/A	#N/A
27.84781	28.03354	28.06564	7	7	49.133	1575800000	CCT7	#N/A	#N/A
29.21803	29.19369	29.15704	19	19	141.11	3790100000	CCT8	#N/A	#N/A
25.43679	25.44714	25.82138	2	2	24.466	397030000	CD59	#N/A	#N/A
27.42454	27.33194	27.67714	4	4	31.318	2672500000	CDH1	#N/A	#N/A
29.3522	29.16907	29.42392	16	16	158.89	4268700000	CERCAM	#N/A	#N/A
27.89342	28.30587	28.46533	2	2	16.093	1980600000	CFL1	#N/A	#N/A
NaN	26.35232	26.53478	6	6	41.07	934250000	PHGDH	#N/A	#N/A
25.89053	NaN	25.86067	3	3	20.406	330700000	CHID1	#N/A	#N/A
31.92476	31.91784	32.03148	20	20	323.31	27773000000	CKAP4	#N/A	#N/A
30.09258	29.68407	29.70905	27	27	197.12	7037500000	CLTC	#N/A	#N/A
29.8269	29.65634	29.70901	17	17	323.31	6512300000	CLU	#N/A	#N/A
27.05258	27.04874	27.2516	5	5	34.394	948810000	CMPK1	#N/A	#N/A
26.12692	26.0975	26.44338	4	4	27.778	476530000	COLGALT2	#N/A	#N/A
29.35628	29.38809	29.65294	24	24	174.45	5735700000	COPA	#N/A	#N/A
27.37227	27.39468	27.34443	8	8	57.849	1121500000	COPB1	#N/A	#N/A
29.37507	28.91701	29.0961	19	19	166.35	4734800000	COPB2	#N/A	#N/A
27.09999	27.21206	27.26356	5	5	37.494	1068900000	COPE	#N/A	#N/A
27.88011	27.79092	27.84452	5	5	40.511	2004400000	COPG1	#N/A	#N/A
25.79124	26.12504	NaN	4	4	28.803	369620000	COX4I1	#N/A	#N/A
NaN	26.14094	26.3582	4	4	26.234	451130000	COX5A	#N/A	#N/A
27.17646	26.98087	27.00785	8	8	56.518	919730000	CPNE1	#N/A	#N/A
28.66034	28.49732	28.59099	4	4	30.451	2540000000	CRP	#N/A	#N/A
NaN	27.56993	27.82742	3	3	22.305	1197100000	CRTAP	#N/A	#N/A
30.4716	29.79551	29.45374	10	10	94.573	6978300000	CRYAB	#N/A	#N/A
27.89741	28.23695	28.06512	8	8	65.16	1973600000	CYB5R3	#N/A	#N/A
25.98235	26.00717	26.42905	5	5	36.617	463380000	CYP20A1	#N/A	#N/A
27.03265	NaN	26.90495	6	6	37.508	745600000	DARS	#N/A	#N/A
28.80104	29	29.03042	7	7	49.739	4142300000	DDOST	#N/A	#N/A
28.18002	28.1821	28.42858	11	9	88.717	2432700000	DDX17	#N/A	#N/A
27.4807	27.51028	27.66614	11	10	65.712	1240400000	DDX3X	#N/A	#N/A
25.78699	NaN	25.78816	5	3	17.743	462450000	DDX5	#N/A	#N/A
32.15777	32.00825	31.77702	32	29	323.31	30683000000	DES	#N/A	#N/A
25.25122	25.15395	25.61248	2	2	14.279	247520000	DHRS4	#N/A	#N/A
29.64349	28.64258	29.31471	19	19	154.79	4473500000	DHX9	#N/A	#N/A
25.32694	NaN	25.61813	3	3	20.489	251240000	DLAT	#N/A	#N/A
26.58864	26.58778	26.7078	5	5	33.428	666670000	DLD	#N/A	#N/A
26.04987	26.28003	26.50927	6	6	40.833	469030000	DLST	#N/A	#N/A
27.2154	26.91957	27.29518	5	5	35.43	1499100000	DPYSL2	#N/A	#N/A
33.27156	33.31352	32.94864	19	19	179.55	75663000000	EEF1A	#N/A	#N/A
27.09909	26.91991	27.05206	5	2	58.286	784700000	EEF1D	#N/A	#N/A
29.96444	29.83348	29.87129	11	11	84.006	7925800000	EEF1G	#N/A	#N/A
31.58679	31.50711	31.56129	32	31	285.65	23747000000	EEF2	#N/A	#N/A
25.10282	NaN	25.23411	4	4	25.045	180380000	EHD2	#N/A	#N/A
27.18234	27.38121	27.17255	6	6	42.795	974910000	EIF2S3	#N/A	#N/A
26.86938	26.66452	27.04656	7	7	40.93	748690000	EIF3A	#N/A	#N/A
26.73324	26.65935	26.59335	5	5	28.817	633480000	EIF3B	#N/A	#N/A

NaN	25.4587	25.59181	3	3	16.279	181300000	EIF3E	#N/A	#N/A
NaN	25.9662	26.22742	3	3	20.737	403240000	EIF3I	#N/A	#N/A
30.4179	30.03708	29.87505	18	8	182.43	7777200000	EIF4A1	#N/A	#N/A
26.05753	NaN	26.42252	3	3	23.483	395500000	ELAVL1	#N/A	#N/A
30.70668	30.60267	30.41397	17	15	312.31	12254000000	ENO1	#N/A	#N/A
28.39354	28.61646	28.66492	4	2	31.89	3502000000	ENO3	#N/A	#N/A
28.55753	28.14967	28.26074	11	11	82.059	2072600000	ENPP1	#N/A	#N/A
26.92128	27.12307	27.53059	9	6	59.219	1078900000	EPRS	#N/A	#N/A
28.62694	28.6326	28.84751	10	8	64.574	2613500000	EPX	#N/A	#N/A
26.87982	26.98348	26.39289	3	3	24.022	746750000	ERP29	#N/A	#N/A
27.54642	27.53118	27.46762	7	7	42.353	1215700000	ERP44	#N/A	#N/A
27.03915	26.59306	NaN	3	3	23.236	605340000	ETFA	#N/A	#N/A
26.46151	26.34885	26.58878	5	5	30.732	547760000	ETFB	#N/A	#N/A
25.03616	25.07333	25.06973	2	2	11.661	214800000	FAM162A	#N/A	#N/A
25.87949	25.44285	25.89537	2	2	19.333	395530000	FAM3C	#N/A	#N/A
30.40466	30.53046	30.7647	29	1	256.14	9664200000	FASN	#N/A	#N/A
28.95374	29.15593	29.4145	3	3	20.557	3696600000	FAU	#N/A	#N/A
26.78768	26.8846	26.96719	3	3	22.672	731400000	FBL	#N/A	#N/A
30.96451	30.98203	31.26746	11	10	99.671	16645000000	FKBP10	#N/A	#N/A
28.10104	28.18485	28.17479	5	5	33.461	1965800000	FKBP11	#N/A	#N/A
27.48401	27.08396	NaN	3	3	27.122	710340000	FKBP7	#N/A	#N/A
30.37555	29.83974	29.72524	12	11	87.956	7753900000	FKBP9	#N/A	#N/A
26.32354	26.31579	26.3304	6	6	46.178	585880000	FLNB	#N/A	#N/A
27.58226	27.33782	27.35951	4	4	23.905	1576500000	FLNC	#N/A	#N/A
26.54218	26.29165	26.57845	4	4	25.919	561030000	FSCN1	#N/A	#N/A
26.23237	26.18208	26.0536	5	5	29.698	501800000	FUBP1	#N/A	#N/A
26.49413	NaN	26.48313	3	3	24.368	507700000	FUS	#N/A	#N/A
28.03228	27.93568	27.93517	7	7	49.994	1953200000	GALE	#N/A	#N/A
30.06766	29.57398	29.60871	23	23	204.23	6940300000	GANAB	#N/A	#N/A
32.92352	33.29885	33.28389	21	19	323.31	78498000000	GAPDH	#N/A	#N/A
26.19378	26.44899	26.21625	6	6	38.774	543470000	GARS	#N/A	#N/A
30.2911	30.19543	30.19554	25	14	205.17	8535100000	GBF1	#N/A	#N/A
28.30348	28.28096	28.37799	6	1	43.349	2192400000	GBI1	#N/A	#N/A
25.71427	25.8148	NaN	9	4	29.635	473930000	GDI1	#N/A	#N/A
28.00089	27.93517	27.89169	10	5	73.41	2562800000	GDI2	#N/A	#N/A
30.38206	29.99981	29.99994	23	1	200.56	8690000000	GFPT1	#N/A	#N/A
28.9955	29.05577	29.36728	15	10	106.54	3606400000	GFPT2	#N/A	#N/A
26.3084	NaN	26.15742	8	8	52.492	834410000	GLG1	#N/A	#N/A
28.44241	28.2208	28.72621	11	11	90.99	2373200000	GLUD1	#N/A	#N/A
NaN	26.02878	26.08829	4	3	20.785	360240000	GNAS	#N/A	#N/A
29.87703	30.03013	30.2732	13	13	129.3	8457300000	GNB2L1	#N/A	#N/A
28.00956	28.29097	28.15325	4	4	29.515	1972100000	GNB3	#N/A	#N/A
28.52294	28.47139	28.77703	10	10	85.308	3169300000	GOT2	#N/A	#N/A
27.28047	27.17864	27.32517	9	9	65.849	1277500000	GPI	#N/A	#N/A
26.05976	NaN	26.42248	5	5	32.683	470220000	GPX7	#N/A	#N/A
25.87138	NaN	26.24603	4	4	26.358	326400000	GPX8	#N/A	#N/A
26.30252	NaN	26.194	4	4	29.995	393290000	GRB2	#N/A	#N/A

31.79153	31.68704	31.7878	29	29	276.11	28153000000	GRP-58	#N/A	#N/A
30.29975	30.28383	30.15316	19	19	202.4	10286000000	GSN	#N/A	#N/A
27.30982	27.57895	27.71188	6	6	45.982	1628700000	H1FX	#N/A	#N/A
32.58791	32.23532	32.04221	5	1	104.75	38764000000	H2AFX	#N/A	#N/A
27.4635	27.49732	27.74458	3	3	17.462	1328300000	H2AFY	#N/A	#N/A
33.72913	33.79042	33.6852	10	10	71.035	1.165E+11	H3F3A	#N/A	#N/A
26.94447	26.84158	27.25997	8	8	50.567	980200000	HADHA	#N/A	#N/A
27.86938	27.78862	28.02237	9	9	76.794	1507800000	HADHB	#N/A	#N/A
33.74595	34.0833	33.84642	10	10	155.19	1.0671E+11	HBA	#N/A	#N/A
35.61998	35.59965	35.27649	16	8	323.31	3.1071E+11	HBB	#N/A	#N/A
27.72754	27.78936	29.00525	15	15	115.23	2626600000	HDLBP	#N/A	#N/A
31.86589	31.90142	32.08423	26	17	323.31	30435000000	HSP90	#N/A	#N/A
31.75127	31.76224	31.9546	17	10	92.793	32376000000	HIST1H1B	#N/A	#N/A
33.43166	33.74845	33.49905	20	7	182.26	1.1772E+11	HIST1H1T	#N/A	#N/A
35.01692	34.96297	34.50912	13	3	214.7	2.1713E+11	HIST1H2BA	#N/A	#N/A
35.33993	35.15285	34.64124	15	15	167.79	2.4993E+11	HIST1H4A	#N/A	#N/A
29.63263	30.99665	30.23375	13	3	21.645	9990000000	HIST3H2BB	#N/A	#N/A
27.49526	27.02612	28.08091	8	8	56.101	1279900000	HK1	#N/A	#N/A
27.67607	27.73518	27.41828	5	5	38.775	1249200000	HMGB1	#N/A	#N/A
25.87893	25.98681	NaN	4	4	35.048	257420000	HNRNPA1	#N/A	#N/A
28.41546	27.88629	28.12045	8	4	68.695	2245500000	HNRNPA2/B1	#N/A	#N/A
27.58054	27.60964	27.11486	5	5	45.785	1187800000	HNRNPA3	#N/A	#N/A
26.34374	26.80292	26.62993	2	2	16.847	605220000	HNRNPC	#N/A	#N/A
27.54525	28.10229	27.78581	4	3	28.333	1489200000	HNRNPH1	#N/A	#N/A
28.33765	28.38451	28.61593	12	12	93.274	2265900000	HNRNPK	#N/A	#N/A
26.52105	26.9015	26.96906	3	3	30.643	723810000	HNRNPL	#N/A	#N/A
29.29883	28.87979	29.39667	15	15	118.35	4537100000	HNRNPM	#N/A	#N/A
29.76574	29.96582	30.08525	17	17	147.87	8575600000	HNRNPU	#N/A	#N/A
26.20193	25.96327	26.22514	3	3	18.278	515490000	HNRNPUL2	#N/A	#N/A
28.45246	28.37811	28.59648	5	5	60.157	2226200000	HP	#N/A	#N/A
26.77102	26.71934	26.83894	5	5	31.218	714550000	HP1BP3	#N/A	#N/A
25.51485	25.12542	25.8235	4	4	42.193	336270000	HSD17B10	#N/A	#N/A
NaN	25.65706	25.92859	5	5	31.041	242730000	HSD17B4	#N/A	#N/A
27.68211	27.5154	27.49732	16	7	115.7	1844000000	HSP70	#N/A	#N/A
32.68685	32.716	32.59877	33	31	323.31	48917000000	HSP90B1	#N/A	#N/A
NaN	28.82086	29.15567	14	4	38.779	3723000000	HSPA2	#N/A	#N/A
32.66732	32.6338	32.41008	34	32	323.31	46947000000	HSPA5	#N/A	#N/A
29.47787	29.88622	29.50156	7	1	11.789	5391700000	HSPA6	#N/A	#N/A
27.96615	28.01839	28.00051	11	11	88.448	1608600000	HSPA9	#N/A	#N/A
30.7198	30.19331	30.6193	16	16	162.89	10002000000	HSPD1	#N/A	#N/A
28.02073	28.01036	28.52526	7	7	46.519	1862300000	HSPE1	#N/A	#N/A
26.22179	25.67853	24.56593	6	5	31.484	366080000	IDH1	#N/A	#N/A
28.78852	28.80603	28.89862	12	11	82.798	2796100000	IDH2	#N/A	#N/A
26.80033	26.52419	26.78144	5	5	34.858	644830000	IDH3A	#N/A	#N/A
25.9376	25.75934	NaN	2	2	12.694	383370000	IGHA	#N/A	#N/A
28.72377	28.80511	28.76765	8	8	84.857	2702000000	IGHD	#N/A	#N/A
30.50815	30.41155	30.68445	9	0	68.35	9845100000	IGHG	#N/A	#N/A

30.91257	31.07508	31.13277	11	1	175.36	13813000000	IGHG	#N/A	#N/A
29.61472	29.48646	29.2656	31	31	323.31	20828000000	IL1RAP	#N/A	#N/A
27.49595	27.21919	27.53934	3	3	25.406	1106400000	ILF2	#N/A	#N/A
26.9968	27.23708	27.0559	5	5	37.931	1214400000	ILF3	#N/A	#N/A
NaN	24.83195	25.58832	3	2	18.756	198340000	IMPDH2	#N/A	#N/A
25.47537	NaN	25.82828	3	3	18.579	238440000	IPO5	#N/A	#N/A
26.90104	26.9327	27.1671	13	13	93.836	1090300000	IQGAP1	#N/A	#N/A
27.31614	27.09235	27.41836	5	5	31.627	983850000	KPNB1	#N/A	#N/A
27.20284	27.85079	27.9571	12	6	120.81	2112900000	KRT1	#N/A	#N/A
NaN	26.00239	26.39568	4	4	28.506	484480000	LAMP1	#N/A	#N/A
24.99404	NaN	24.73862	4	4	25.698	162370000	LCP1	#N/A	#N/A
30.8915	30.94391	31.01611	15	13	126.1	17606000000	LDHA	#N/A	#N/A
28.23512	28.20992	28.33947	8	3	44.76	2986600000	LDHB	#N/A	#N/A
30.94224	30.72477	30.88881	5	5	50.349	24717000000	LECT2	#N/A	#N/A
25.54834	25.59092	25.5501	2	2	16.133	296420000	LMAN2	#N/A	#N/A
30.41246	30.3911	30.37171	30	1	288.53	13692000000	LMNA	#N/A	#N/A
27.48884	27.47011	27.24291	8	7	48.213	1104500000	LMNB1	#N/A	#N/A
24.72718	NaN	24.87056	4	3	18.431	150120000	LMNB2	#N/A	#N/A
31.88718	31.83579	31.72106	15	0	301.26	28470000000	LOC100127131	#N/A	#N/A
32.27673	32.16414	31.80505	15	6	45.068	26403000000	LOC100154783	#N/A	#N/A
25.8877	NaN	25.80003	2	2	11.562	342840000	LOC100155889	#N/A	#N/A
26.77568	NaN	26.41901	7	2	34.832	606460000	LOC100156325	#N/A	#N/A
33.511	33.56898	33.36202	27	27	323.31	86014000000	LOC100156689	#N/A	#N/A
NaN	26.14009	26.26293	5	5	36.854	435880000	LOC100157249	#N/A	#N/A
37.52262	36.05809	35.82691	4	4	207.32	7.9947E+11	LOC100302368	#N/A	#N/A
29.51232	29.23396	29.77057	9	9	74.431	9184200000	LOC100510904	#N/A	#N/A
25.06443	25.56863	NaN	2	2	16.152	200270000	LOC100511690	#N/A	#N/A
25.66139	25.54416	25.64678	4	4	25.749	340520000	LOC100512253	#N/A	#N/A
26.7986	NaN	26.79067	3	3	17.52	579800000	LOC100512637	#N/A	#N/A
28.46673	28.48097	28.66729	9	9	91.985	2577600000	LOC100513892	#N/A	#N/A
32.43378	32.38105	32.43966	15	10	177.45	36297000000	LOC100514666	#N/A	#N/A
30.18553	30.13931	30.25586	9	9	55.756	9409000000	LOC100516261	#N/A	#N/A
30.24728	29.86729	29.87935	23	1	252.87	7078000000	LOC100516776	#N/A	#N/A
30.63027	30.48894	30.61404	7	7	68.388	11384000000	LOC100517228	#N/A	#N/A
26.53662	NaN	26.36885	4	4	27.646	629210000	LOC100517744	#N/A	#N/A
28.62006	28.31713	28.66166	10	10	90.457	3364900000	LOC100518254	#N/A	#N/A
26.31771	26.31237	26.67949	4	4	28.063	544100000	LOC100518399	#N/A	#N/A
28.99213	28.8966	28.8328	11	11	93.326	3713100000	LOC100519984	#N/A	#N/A
30.15473	29.79314	29.8419	8	8	123.1	6266500000	LOC100521468	#N/A	#N/A
28.37559	28.12465	28.37455	4	4	64.337	2019600000	LOC100523213	#N/A	#N/A
29.02398	28.85807	28.41921	4	4	28.881	3077000000	LOC100523526	#N/A	#N/A
27.70074	28.04338	28.16868	3	3	29.28	1561700000	LOC100523801	#N/A	#N/A
29.74562	29.74674	29.9806	5	5	33.773	9254800000	LOC100523846	#N/A	#N/A
27.46684	27.702	27.72936	4	4	36.417	1240500000	LOC100524170	#N/A	#N/A
26.50127	27.4419	27.37435	2	2	13.207	851300000	LOC100524880	#N/A	#N/A
26.23478	26.05641	26.33028	8	2	70.549	597780000	LOC100525988	#N/A	#N/A
27.03612	26.51281	26.63492	8	2	13.903	859850000	LOC100526167	#N/A	#N/A

30.41094	30.49534	30.41488	8	8	70.409	9378000000	LOC100620439	#N/A	#N/A
27.1029	27.22784	27.48424	5	3	41.062	956810000	LOC100620941	#N/A	#N/A
26.49945	26.34272	26.78918	14	3	42.832	617770000	LOC100621981	#N/A	#N/A
29.85441	30.12817	30.10487	12	12	164.47	6514100000	LOC100622330	#N/A	#N/A
NaN	26.93078	27.67674	17	3	36.604	911570000	LOC100623583	#N/A	#N/A
29.13506	29.18307	29.06252	5	5	51.604	3589000000	LOC100623679	#N/A	#N/A
NaN	24.5373	25.47649	3	3	20.356	155740000	LOC100623684	#N/A	#N/A
30.21071	30.37472	30.45865	9	9	63.036	10171000000	LOC100623913	#N/A	#N/A
28.81821	28.82259	29.19934	6	6	37.585	3071800000	LOC100624417	#N/A	#N/A
29.20886	29.4109	29.17229	6	6	39.68	4363500000	LOC100624537	#N/A	#N/A
31.02723	30.95913	31.17075	2	2	19.775	13163000000	LOC100625180	#N/A	#N/A
24.77761	24.99606	24.80307	2	2	27.683	186160000	LOC100626266	#N/A	#N/A
30.87826	30.78994	30.87547	12	12	126.82	18367000000	LOC100626701	#N/A	#N/A
28.39938	27.83593	26.3784	10	10	69.362	8739200000	LOC100737120	#N/A	#N/A
24.4431	NaN	25.28718	3	3	19.594	151940000	LOC100737246	#N/A	#N/A
27.47205	27.8951	28.17617	11	11	74.667	1495600000	LOC100737407	#N/A	#N/A
31.19143	31.13492	30.93157	9	8	89.431	16435000000	LOC100737553	#N/A	#N/A
32.8752	32.9347	32.82758	15	6	264.78	57354000000	LOC100737887	#N/A	#N/A
26.63437	26.07938	26.4654	5	5	41.55	592510000	LOC100737962	#N/A	#N/A
30.57073	30.55536	30.70074	13	13	107.33	11447000000	LOC100738304	#N/A	#N/A
27.75066	27.81592	28.04129	8	8	50.388	1464900000	LOC100738388	#N/A	#N/A
26.42707	26.09603	25.65704	2	2	15.113	853750000	LOC100738863	#N/A	#N/A
26.49063	26.21098	NaN	2	2	15.116	553810000	LOC100739851	#N/A	#N/A
27.37592	27.62303	27.5755	3	3	18.726	1239600000	LOC102163847	#N/A	#N/A
29.39387	29.33089	29.39204	6	6	70.58	5517200000	LOC102164134	#N/A	#N/A
28.23594	28.3006	27.89481	1	1	6.9641	2455200000	LOC102165647	#N/A	#N/A
31.19372	30.80878	30.48731	14	14	220.35	22820000000	LOC102165939	#N/A	#N/A
26.86231	26.72273	26.21095	4	4	28.54	643750000	LOC494560	#N/A	#N/A
29.94182	29.69495	29.86366	18	5	43.179	9224400000	LOC595122	#N/A	#N/A
27.41296	27.31959	27.06312	4	4	56.415	1036300000	LOC733637	#N/A	#N/A
NaN	25.44168	25.30159	4	4	36.356	452930000	LPL	#N/A	#N/A
28.62808	28.52548	28.70777	27	27	193.17	3279400000	LRP1	#N/A	#N/A
28.07005	27.83599	27.77605	7	6	83.746	1553700000	LTF	#N/A	#N/A
29.09126	29.74549	29.96279	16	3	82.218	13295000000	LYZ	#N/A	#N/A
27.53356	27.41321	27.7649	14	2	46.004	1199000000	LYZ	#N/A	#N/A
31.90638	31.61824	31.91528	16	4	323.31	64996000000	LYZ3	#N/A	#N/A
NaN	25.053	25.29674	2	2	14.209	231610000	MAGT1	#N/A	#N/A
27.47383	27.03507	26.55476	4	4	35.543	943520000	MATR3	#N/A	#N/A
27.06897	26.76053	26.94715	4	4	29.228	784420000	MDH1	#N/A	#N/A
27.79476	27.74663	27.79092	9	8	61.683	1486700000	ME1	#N/A	#N/A
26.7433	26.78506	26.93809	9	9	70.856	1455300000	MFI2	#N/A	#N/A
25.86186	NaN	25.50425	2	2	15.921	262650000	MIF	#N/A	#N/A
26.83316	26.63312	26.98131	7	5	32.403	680460000	MPO	#N/A	#N/A
30.23968	30.08297	30.12866	20	11	141.37	8078400000	MSN	#N/A	#N/A
25.42621	NaN	25.34133	3	3	17.271	198150000	MYH1	#N/A	#N/A
30.19742	29.54222	29.96513	31	21	234.22	6612200000	MYH9	#N/A	#N/A
29.46059	29.50465	29.71204	5	5	70.046	5327000000	MYL6	#N/A	#N/A

25.87242	25.55271	25.78848	2	2	11.561	334350000	MYO1B	#N/A	#N/A
25.97496	25.32656	25.70406	4	4	27.518	475620000	MYO1C	#N/A	#N/A
26.59377	26.69763	NaN	2	1	14.791	516980000	NAP1L4	#N/A	#N/A
25.82355	25.68985	25.8541	4	4	42.651	329920000	NAPA	#N/A	#N/A
25.65499	NaN	25.60065	2	2	12.55	257540000	NDUFS1	#N/A	#N/A
30.13638	30.08639	30.00517	8	4	61.131	8499500000	NME2	#N/A	#N/A
28.73434	28.64667	28.81693	1	1	7.4825	3134600000	NME3	#N/A	#N/A
28.27742	28.26096	28.60368	9	9	63.917	2305600000	NONO	#N/A	#N/A
28.60791	28.31268	28.02041	6	6	39.847	2721500000	NPM1	#N/A	#N/A
24.75807	NaN	24.78517	3	3	17.499	159610000	NT5E	#N/A	#N/A
26.9257	26.92366	27.02422	8	7	60.867	862880000	NUCB1	#N/A	#N/A
29.59267	29.57124	29.64709	16	16	152.03	5872600000	OAT	#N/A	#N/A
24.72281	24.96243	NaN	2	2	12.865	175390000	OLA1	#N/A	#N/A
25.95782	26.29063	26.12445	3	3	21.147	430970000	ORM1	#N/A	#N/A
33.93649	33.9948	33.79401	35	35	323.31	1.1865E+11	P4HB	#N/A	#N/A
29.09053	28.48719	29.16572	14	9	142.81	3284900000	PABPC1	#N/A	#N/A
25.87881	25.70564	25.95067	8	3	21.736	380010000	PABPC4	#N/A	#N/A
27.42414	26.59918	26.51399	8	7	50.692	1043500000	PAPSS1	#N/A	#N/A
31.82608	31.65284	31.76268	25	24	214.19	27433000000	PAPSS2	#N/A	#N/A
24.48726	NaN	24.25875	3	3	19.748	107110000	PARP1	#N/A	#N/A
25.8305	25.7263	NaN	4	2	14.702	321930000	PCBP2	#N/A	#N/A
31.27991	31.23957	31.3408	31	31	282.8	19455000000	PDIA4	#N/A	#N/A
29.63663	29.78269	29.93438	13	13	184.03	8820900000	pdi-p5	#N/A	#N/A
26.79947	26.83135	27.06815	3	3	22.134	813580000	PEBP1	#N/A	#N/A
27.39411	27.34942	27.48378	11	8	76.408	1665000000	PFKL	#N/A	#N/A
27.33219	27.19235	27.54495	13	11	107.3	1649000000	PFKP	#N/A	#N/A
28.50158	28.77737	28.50506	7	7	71.709	2502200000	PFN1	#N/A	#N/A
29.64234	29.40532	29.39356	12	12	138.61	7244700000	PGAM1	#N/A	#N/A
30.4981	30.03354	30.44431	22	0	237.22	12687000000	PGK1	#N/A	#N/A
25.18492	NaN	25.43463	3	3	21.452	233350000	PGRMC2	#N/A	#N/A
27.76129	27.90805	28.19653	7	7	59.593	1558600000	PHB2	#N/A	#N/A
29.2151	29.13545	29.22867	8	8	57.028	3655000000	PHOSPHO1	#N/A	#N/A
31.50744	31.05388	31.38515	18	18	188.41	29736000000	PKLR	#N/A	#N/A
26.63824	26.49323	26.8334	5	4	35.279	803740000	PLCD1	#N/A	#N/A
27.91553	27.80839	27.91741	23	22	146.84	1556200000	PLEC	#N/A	#N/A
29.77582	29.62643	29.54793	6	1	132.72	5029100000	PMAP23	#N/A	#N/A
26.64883	26.83244	26.75659	6	6	38.168	691680000	PPP2R1A	#N/A	#N/A
30.01691	29.86614	29.88434	8	5	49.279	6868200000	PRDX1	#N/A	#N/A
28.49179	28.35825	28.34452	6	6	42.555	2883900000	PRDX2	#N/A	#N/A
27.17769	27.11763	27.07327	5	5	35.659	891250000	PRDX3	#N/A	#N/A
30.13504	30.56438	30.05634	10	7	86.057	10038000000	PRDX4	#N/A	#N/A
25.97895	NaN	26.26327	6	6	40.881	1882500000	PRDX6	#N/A	#N/A
28.76563	28.89954	28.68852	11	11	130.81	3223100000	PRKCSH	#N/A	#N/A
29.63223	29.83186	29.70603	8	8	80.811	5148600000	PROC	#N/A	#N/A
NaN	26.43567	26.78967	3	3	24.862	518380000	PRTN3	#N/A	#N/A
26.44643	25.57594	25.65261	3	3	22.07	438510000	PSMA6	#N/A	#N/A
25.86093	25.84352	NaN	2	2	13.873	357400000	PSMB4	#N/A	#N/A

25.79054	NaN	25.76142	3	3	20.306	280430000	PSMD11	#N/A	#N/A
25.44364	25.27092	NaN	3	3	20.181	273120000	PSMD14	#N/A	#N/A
NaN	24.72583	25.56465	4	4	27.577	241680000	PSMD2	#N/A	#N/A
26.84577	27.1208	27.49587	5	5	29.593	941920000	PTBP1	#N/A	#N/A
26.47994	26.26696	26.38181	6	6	36.445	536240000	PTK7	#N/A	#N/A
25.97042	25.96506	26.13457	4	4	24.293	435180000	PURA	#N/A	#N/A
27.22343	27.22186	27.43516	13	13	79.427	1036600000	PYGB	#N/A	#N/A
26.81885	26.91843	26.99658	5	5	29.603	776980000	RAB11A	#N/A	#N/A
NaN	26.06632	26.19043	5	5	31.979	335520000	RAB18	#N/A	#N/A
NaN	27.03999	27.44806	3	3	28.864	846540000	RAB39A	#N/A	#N/A
25.58124	25.71301	25.79702	2	2	18.08	331690000	RALY	#N/A	#N/A
29.10247	29.21155	29.07948	10	10	74.396	4235300000	RAN	#N/A	#N/A
27.70682	27.87156	27.96719	2	2	14.053	1496500000	RAP1A	#N/A	#N/A
27.94648	27.8282	27.50499	5	5	45.408	2722700000	RARRES2	#N/A	#N/A
26.44664	26.54181	26.62185	4	4	37.454	607560000	RBMX	#N/A	#N/A
28.7303	28.80372	28.40272	10	10	86.596	3080800000	RCN1	#N/A	#N/A
30.14783	30.23478	30.06201	8	8	142.03	8716200000	RCN3	#N/A	#N/A
27.51503	27.70589	27.86508	4	4	33.413	1397900000	RHOA	#N/A	#N/A
30.18778	29.25311	29.30843	8	8	163.62	10890000000	RNASE4	#N/A	#N/A
30.64272	30.30149	30.18542	11	11	145.69	11088000000	RPL10	#N/A	#N/A
29.49072	29.27026	29.31023	7	2	64.965	5413100000	RPL10A	#N/A	#N/A
29.3538	29.48955	29.48871	10	10	108.75	5713200000	RPL11	#N/A	#N/A
30.13638	30.2589	30.509	8	8	80.759	10270000000	RPL13	#N/A	#N/A
29.86796	30.08411	30.28339	13	13	80.826	8108200000	RPL13A	#N/A	#N/A
28.16677	28.41961	28.267	4	4	33.359	2117000000	RPL17	#N/A	#N/A
30.83334	30.91257	30.86267	7	7	108.74	15583000000	RPL18	#N/A	#N/A
30.6501	30.49219	30.27197	11	11	78.765	10878000000	RPL18A	#N/A	#N/A
29.7891	29.38332	29.4245	5	5	68.931	5758500000	RPL19	#N/A	#N/A
30.09597	30.14224	30.20466	7	7	66.002	7672100000	RPL21	#N/A	#N/A
29.97774	30.10837	30.22481	7	6	63.332	8971600000	RPL22	#N/A	#N/A
28.28109	27.83352	28.48623	3	3	21.804	2315600000	RPL23	#N/A	#N/A
30.26282	30.12016	30.03078	9	9	64.07	7681600000	RPL23A	#N/A	#N/A
29.92804	29.76538	29.91171	5	5	36.69	6580800000	RPL24	#N/A	#N/A
28.92198	28.68281	28.45509	11	11	70.039	3001200000	RPL26	#N/A	#N/A
29.82611	29.78761	29.74774	8	8	63.301	6320600000	RPL27	#N/A	#N/A
28.4739	28.61894	28.54893	4	4	34.297	2393100000	RPL29	#N/A	#N/A
30.58289	30.3909	30.29909	17	17	135.71	12049000000	RPL3	#N/A	#N/A
29.03554	28.78516	28.9884	7	7	60.51	3751600000	RPL30	#N/A	#N/A
28.24776	28.19009	28.3362	4	4	24.16	1914200000	RPL34	#N/A	#N/A
31.4515	31.21616	31.11923	22	10	186.3	17135000000	RPL4	#N/A	#N/A
30.17379	30.23945	29.92649	10	10	88.252	8693100000	RPL5	#N/A	#N/A
32.62061	32.32254	32.56844	18	18	225.46	40983000000	RPL6	#N/A	#N/A
30.83349	30.65284	31.00979	14	7	108.18	13182000000	RPL7	#N/A	#N/A
30.32732	30.48769	30.54176	6	6	48.737	11490000000	RPL7A	#N/A	#N/A
31.34884	31.33431	31.59081	13	13	98.211	19941000000	RPL8	#N/A	#N/A
29.7756	29.86024	29.67813	6	6	44.379	6601000000	RPL9	#N/A	#N/A
29.70999	29.11078	29.38245	8	8	79.191	5270300000	RPLP0	#N/A	#N/A

29.87976	29.83882	29.74934	17	17	134.04	7482500000	RPN1	#N/A	#N/A
30.52999	30.53278	30.60231	14	14	99.938	11454000000	RPS11	#N/A	#N/A
28.81268	28.76452	29.07844	3	3	19.956	3285300000	RPS12	#N/A	#N/A
28.77165	28.55076	28.65612	6	6	45.377	3466200000	RPS13	#N/A	#N/A
30.78784	30.88925	30.57822	12	12	91.65	14745000000	RPS16	#N/A	#N/A
29.65971	29.68351	29.85131	3	3	21.802	5780300000	RPS17	#N/A	#N/A
30.48961	30.55655	30.75613	12	12	83.13	12547000000	RPS2	#N/A	#N/A
28.65683	28.78066	28.99949	4	4	32.479	4437700000	RPS20	#N/A	#N/A
27.00389	27.42486	27.64595	2	2	16.053	1034500000	RPS21	#N/A	#N/A
30.8097	30.60311	30.70594	6	6	53.499	11253000000	RPS25	#N/A	#N/A
29.40621	29.45488	29.58606	4	4	40.246	5027600000	RPS27	#N/A	#N/A
28.2539	27.64423	27.28833	3	3	27.718	1331500000	RPS27A	#N/A	#N/A
30.97972	31.14096	30.97965	21	21	172.52	15605000000	RPS3	#N/A	#N/A
31.07954	31.1098	31.24921	18	18	141.28	17611000000	RPS3A	#N/A	#N/A
31.62139	31.39397	31.23928	16	16	157.93	21434000000	RPS4	#N/A	#N/A
29.47605	29.43078	29.5349	8	8	86.23	5280900000	RPS5	#N/A	#N/A
30.91648	30.86142	30.77172	15	7	124.15	13145000000	RPS6	#N/A	#N/A
29.47667	29.44969	29.63843	6	6	39.632	5340800000	RPS7	#N/A	#N/A
30.36234	30.37192	30.18601	13	13	179.15	11049000000	RPS8	#N/A	#N/A
NaN	28.24504	28.05455	13	2	13.079	1160700000	RPS9	#N/A	#N/A
30.30932	30.36286	30.28273	13	2	85.755	9704400000	RPS9	#N/A	#N/A
29.16591	29.69428	29.71362	11	11	149.77	4991100000	RPSA	#N/A	#N/A
30.26539	30.39826	30.42902	26	26	234.95	9770500000	RRBP1	#N/A	#N/A
27.23178	27.2498	27.47723	11	11	73.16	1141100000	RTCB	#N/A	#N/A
27.70589	27.7916	NaN	5	5	35.971	967330000	SAR1A	#N/A	#N/A
28.88629	28.9305	29.05719	13	13	123.39	4748600000	SCIN	#N/A	#N/A
27.31354	27.3652	27.34113	7	7	51.334	1028800000	SDHA	#N/A	#N/A
25.6216	25.74291	NaN	2	2	13.122	309750000	SEC11A	#N/A	#N/A
25.30239	NaN	25.46588	2	2	21.327	264940000	SEC13	#N/A	#N/A
27.16749	26.879	27.12751	9	8	75.475	1091000000	SEC23A	#N/A	#N/A
27.31691	27.30269	27.45537	7	7	56.494	1174900000	SEC24D	#N/A	#N/A
27.12485	26.89908	27.57838	7	7	44.03	1091900000	SEC31A	#N/A	#N/A
NaN	28.42198	28.75411	2	2	17.039	1897500000	SEC61B	#N/A	#N/A
26.64609	26.91798	26.49974	5	5	32.853	819690000	SEPT9	#N/A	#N/A
29.56491	29.29263	29.36967	12	9	89.982	4296600000	SERPINA3-2	#N/A	#N/A
27.08679	26.92479	27.18272	5	5	37.343	820270000	SLC25A1	#N/A	#N/A
28.02844	28.18154	28.37206	7	7	48.959	1734700000	SLC25A3	#N/A	#N/A
30.68913	30.77635	30.9685	9	3	60.283	11981000000	SLC25A6	#N/A	#N/A
26.78918	26.73104	27.26973	6	6	48.27	733530000	SMPD3	#N/A	#N/A
28.91957	28.91789	29.01398	14	14	102.05	3767200000	SND1	#N/A	#N/A
27.10239	26.91696	26.88902	5	5	30.484	800790000	SNRNP70	#N/A	#N/A
24.94244	NaN	25.14503	2	2	13.12	183880000	SNRPA	#N/A	#N/A
28.82177	28.69122	28.89709	7	7	80.896	2874000000	SPP2	#N/A	#N/A
25.02606	24.81436	NaN	2	2	12.498	183870000	SRM	#N/A	#N/A
26.67546	26.53623	26.59648	5	5	29.108	603010000	SRPR	#N/A	#N/A
NaN	25.87526	26.26093	3	3	17.241	310390000	SRPRB	#N/A	#N/A
27.13604	27.0878	27.19366	3	3	22.717	854350000	SSB	#N/A	#N/A

28.29413	28.29079	28.43535	2	2	13.358	2175700000	SSR1	#N/A	#N/A
28.97678	28.75538	28.41973	4	4	34.982	3151900000	SSR4	#N/A	#N/A
25.59537	26.16984	26.14587	4	4	38.031	416210000	ST13	#N/A	#N/A
28.39444	28.4251	28.72481	8	7	54.654	2382800000	STT3A	#N/A	#N/A
24.42675	NaN	24.21416	2	2	12.402	94824000	SUB1	#N/A	#N/A
27.37368	27.21771	27.59106	2	2	13.998	1251200000	SURF4	#N/A	#N/A
27.06157	27.15422	27.27684	5	3	44.551	1009800000	SYNCRIP	#N/A	#N/A
26.74727	26.54346	26.80907	4	4	30.961	651880000	TBL2	#N/A	#N/A
28.3782	28.38784	29.0004	11	11	75.793	2723700000	TCP1	#N/A	#N/A
25.48253	26.05922	25.9018	2	2	19.269	346700000	TECR	#N/A	#N/A
29.32862	29.44743	29.44269	16	15	124.99	4147600000	TF	#N/A	#N/A
28.54292	28.43289	28.40864	13	13	98.54	3383500000	TKT	#N/A	#N/A
28.37534	28.32569	28.18674	18	18	118.69	2071600000	TLN1	#N/A	#N/A
NaN	25.97158	25.99155	2	2	12.075	306880000	TM9SF3	#N/A	#N/A
28.71702	28.59833	28.51164	5	5	39.731	3811200000	TMED10	#N/A	#N/A
27.06219	26.84577	26.99863	3	3	24.051	794360000	TMED2	#N/A	#N/A
26.45249	27.12623	27.07449	3	3	37.348	789980000	TMED9	#N/A	#N/A
26.07995	NaN	25.91962	2	2	15.065	432410000	TMEM43	#N/A	#N/A
28.98027	28.6514	28.67956	9	9	116.04	3631600000	TPI1	#N/A	#N/A
26.56977	26.07971	25.94726	5	5	36.861	487290000	TPM1	#N/A	#N/A
27.81146	27.1489	27.93511	4	4	39.803	1502100000	TPT1	#N/A	#N/A
26.49747	26.39682	25.73368	4	4	32.818	461470000	TRPV4	#N/A	#N/A
32.10465	32.01292	32.16447	17	2	263.11	33599000000	TUBB	#N/A	#N/A
27.36135	27.58606	27.68372	7	7	46.529	1177400000	TUFM	#N/A	#N/A
31.10961	31.04179	31.37124	20	20	268.3	17166000000	UGDH	#N/A	#N/A
27.60031	27.8381	28.08816	16	16	121.36	2597000000	UGP2	#N/A	#N/A
26.99873	NaN	27.40519	4	4	25.169	807460000	UQCRC1	#N/A	#N/A
27.6231	27.30025	27.95964	7	7	47.691	1300800000	VDAC1	#N/A	#N/A
29.21491	29.29483	29.59587	7	7	73.542	4733800000	VDAC2	#N/A	#N/A
27.37542	27.29929	27.31614	9	9	68.96	1022000000	WDR1	#N/A	#N/A
26.68445	26.46641	26.8839	9	9	68.728	681990000	XYLT1	#N/A	#N/A
27.52783	27.15846	26.94592	7	2	42.662	1175400000	YWHAB	#N/A	#N/A
28.03585	27.95394	28.16787	6	6	42.696	1669000000	YWHAE	#N/A	#N/A
NaN	25.65597	25.76552	7	4	29.143	556970000	YWHAG	#N/A	#N/A
27.82366	27.68612	27.87033	7	5	128.12	1643100000	YWHAZ	#N/A	#N/A
32.27436	32.2434	32.12325	4	4	38.913	33554000000	Uncharacterized	#N/A	#N/A
31.95102	31.89291	31.43301	24	15	247.17	26045000000	Uncharacterized	#N/A	#N/A
NaN	26.56763	25.95356	3	3	32.428	573920000	Uncharacterized	#N/A	#N/A
25.93997	26.16411	25.69163	2	2	26.854	392540000	Uncharacterized	#N/A	#N/A
32.5177	32.23732	32.31503	12	12	162.18	40411000000	Uncharacterized	#N/A	#N/A
26.78656	26.38722	NaN	6	3	23.694	526620000	Uncharacterized	#N/A	#N/A
32.27689	32.31141	32.21289	14	14	159.62	40425000000	Uncharacterized	#N/A	#N/A